



HAL
open science

A semi-parametric distribution stitch based on the Berk-Jones test for French daily precipitation bias correction

Philippe Ear, Elena Di Bernardino, Thomas Laloë, Magali Troin, Adrien Lambert

► To cite this version:

Philippe Ear, Elena Di Bernardino, Thomas Laloë, Magali Troin, Adrien Lambert. A semi-parametric distribution stitch based on the Berk-Jones test for French daily precipitation bias correction. 2024. hal-04711389

HAL Id: hal-04711389

<https://hal.science/hal-04711389v1>

Preprint submitted on 26 Sep 2024

HAL is a multi-disciplinary open access archive for the deposit and dissemination of scientific research documents, whether they are published or not. The documents may come from teaching and research institutions in France or abroad, or from public or private research centers.

L'archive ouverte pluridisciplinaire **HAL**, est destinée au dépôt et à la diffusion de documents scientifiques de niveau recherche, publiés ou non, émanant des établissements d'enseignement et de recherche français ou étrangers, des laboratoires publics ou privés.

A semi-parametric distribution stitch based on the Berk-Jones test for French daily precipitation bias correction

Ear Philippe^{1,2*}, Di Bernardino Elena², Laloë Thomas²,
Troin Magali¹, Lambert Adrien¹

¹ Hydroclimat, Aubagne, 13100, France.

² Université Côte d'Azur, Laboratoire J.A. Dieudonné, UMR CNRS
7351, Nice, 06108, France.

*Corresponding author(s). E-mail(s): philippe.ear@hydroclimat.com;
Contributing authors: elena.di_bernardino@unice.fr;
thomas.laloe@unice.fr; magali.troin@hydroclimat.com;
adrien.lambert@hydroclimat.com;

Abstract

Modelling daily precipitation data in a large territory is a complex issue due to its asymmetric distribution with few and spatially sparse extremes. Most parametric distributions fail to model rainfall correctly over a large area, and many impact studies use the non-parametric empirical distribution instead of parametric ones, preferring the robustness of the model on the observed data to the extrapolation to unobserved extremes. In the present paper, we built a distributional semi-parametric model for the bias correction of the ERA5-Land reanalysis using the CERRA-Land reanalysis. The proposed inference procedure is constructed as follows. Firstly, we fit an Extended Generalized Pareto (EGP) distribution to the data. These EGP models give a Generalized Pareto distribution in the upper tail while allowing greater flexibility in the lower one. Secondly, for each location, using an adapted version of the Berk-Jones (BJ) statistical test, we propose to replace a portion of the EGP distribution with either the empirical distribution or an eventually lighter-tail parametric distribution such as the Exponentiated Weibull (ExpW) distribution. The final obtained model is a stitch between the EGP, ExpW and the empirical distributions. The proposed semi-parametric stitch model has been evaluated in a bias correction context against classical pure parametric quantile mapping based on Gamma, ExpW and EGP distributions.

001
002
003
004
005
006
007
008
009
010
011
012
013
014
015
016
017
018
019
020
021
022
023
024
025
026
027
028
029
030
031
032
033
034
035
036
037
038
039
040
041
042
043
044
045
046

047 Comparisons to other classical models show a reduction of the mean absolute
048 and extreme error metrics, especially by removing outliers.

049 **Keywords:** Bias correction, Extreme value theory, Goodness-of-Fit, Parametric
050 distribution, Precipitation modelling

051

052

053

054

055

1 Introduction

056

057

058

1.1 On the bias correction literature: a focus on heavy-tail precipitations

059

060

061

062

063

064

065

066

067

068

069

070

071

072

073

074

075

076

077

078

079

080

081

082

083

084

085

086

087

088

089

090

091

092

Precipitation is one of the main input variables of hydrological models and processes, where heavy rainfall produces catastrophic events with large economic and human impact (Carrió et al., 2022; Costache and Tien Bui, 2020). Extreme Value Theory (EVT) is well suited for modelling extreme hydrological events, especially when it comes to flood events (Katz, 2002). EVT allows for distributions to fit block maxima data in random samples for fixed intervals and to model heavy-tailed data (more details on EVT can be found in De Haan and Ferreira (2006)). Accurate and high-resolution daily precipitation data, especially on extremes, are crucial to correctly calibrate models, forecast floods and contain natural catastrophes (Alfieri and Thielen, 2015; Sangati and Borga, 2009).

However, most available global or continental datasets do not have a high enough resolution (Soares and Cardoso, 2018) for most local impact studies (Henckes et al., 2018), or to represent correctly the extremes (Prein et al., 2016) due to the presence of significant bias, and need to be downscaled and bias corrected (Şan et al., 2023; Cucchi et al., 2020; Xu et al., 2015).

The most popular method for bias correction is the quantile mapping (Lafon et al., 2013) based on the pure empirical distribution in a univariate context. The non-parametric distribution is widely adopted since it does not require any distributional model assumption. However, the corrected values are limited to the reference-period observed ones, thus new extreme events can not be extrapolated or predicted correctly because they result from arbitrary workarounds (Déqué, 2007). Let x_{obs} be the reference time series, considered to have no bias and x_{mod} a time series produced by a biased model that must be corrected. The empirical quantile mapping method can then be described as:

$$x_{\text{mod}}^{\text{corr}} = F_{n,\text{obs}}^{-1}(F_{n,\text{mod}}(x_{\text{mod}})), \quad (1.1)$$

where we use the notation $F_{n,\text{data}}$ for the empirical cumulative distribution function built on the sample `data` of size n , $F_{n,\text{data}}^{-1}$ for the associated quantile function (`data` can be referring to `obs` and `mod` here) and $x_{\text{mod}}^{\text{corr}}$ is the bias corrected model data.

In this study, the main focus is on the distributional fitting required in Equation (1.1). The derived bias correction application is mostly an illustration of the performance of the proposed stitch distribution instead of the empirical one. A deeper bias correction

comparison, for longer time series, is discussed as an interesting future perspective in Section 5 of this paper.

Parametric distributions have also been studied extensively for daily precipitation modelling, with the Gamma distribution (Martinez-Villalobos and Neelin, 2019), a mixture of Generalized Pareto (GP) distribution (Li et al., 2021) or the Extended Generalized Pareto (EGP) distribution (Naveau et al., 2016) (see Equation (B.1) for a precise definition). The light-tailed Gamma distribution fails to represent rainfall in locations with heavy-tail precipitations, better fitted for instance by an ExpW or a GP distribution which can both belong in the maximum Fréchet domain of attraction given the appropriate parameters (Blain and Meschiatti, 2015; Vlček and Huth, 2009). In particular, the GP distribution is the classical precipitation used in the peak-over-threshold models (*i.e.*, based on exceedances) (Rootzén and Tajvidi, 1997; McNeil et al., 1997) and is also often used in extreme precipitation and flood modelling (Yue et al., 2022; Acero et al., 2011). However, the need for a data-driven automatic threshold selection makes it very computationally intensive when the area of interest becomes large or with a highly-resoluted spatial data set. The selection of the threshold is the main issue regarding the GP distribution. To overcome this calibration threshold issue, the EGP distribution class has been developed and allows to model both lower and upper heavy tails (Gamet and Jalbert, 2022; Tencaliec et al., 2019; Naveau et al., 2016) without the need to select a threshold.

While this new distribution class may appropriately fit in some locations, it is not satisfactory everywhere when the study covers a geographically large and resoluted area. In the present work, we propose a method to produce a novel semi-parametric distributional model based on an adapted version of the Berk-Jones (BJ) statistical test (Berk and Jones, 1979; Moscovich et al., 2016). The proposed inference procedure on the considered daily French precipitations will produce a final stitch between the heavy-tailed EGP, the lighter-tailed ExpW and the empirical distribution function. More precisely:

- (i) We fit the EGP distribution on each location;
- (ii) Based on the adapted BJ statistical test, the upper and lower tails are eventually replaced by the ExpW distribution;
- (iii) Finally, if neither parametric distribution was satisfactory enough, the empirical distribution F_n is used.

This mixture of non-parametric and parametric distribution is often called a semi-parametric approach in the literature while combining multiple parametric distributions is referred to as a stitch or a spliced distribution. In this article, we will refer to this as a semi-parametric stitch distribution.

Structure of the paper. In Section 1.2, we present the datasets of daily rainfall over France used in this paper and highlight the need for bias correction. Section 2 describes the proposed semi-parametric distributional model. In Section 3, we apply our method in a case study on the considered reanalysis ERA5-Land (ERA5-L) and CERRA-Land (CERRA-L). Fit and bias correction results are presented in Section 4 with

139 the bias correction of ERA5-L using CERRA-L. Conclusion and key points are dis-
140 cussed in Section 5. The considered metrics are presented in Appendix A and used
141 classical parametric distributions are recalled in Appendix B. Details on the mono-
142 tonicity correction of the proposed stitch distributional model are given in Appendix
143 C. Supplementary figures are available in Appendix D.

144

145 1.2 Bias correction importance on the considered daily 146 precipitations using the ERA5-Land and CERRA-Land 147 datasets 148

149 The whole of metropolitan France is used in this daily precipitation study which cov-
150 ers around 550000 km². To perform bias correction and assess the performance of the
151 new method, a pseudo-observational and a to-be-corrected-model dataset are needed,
152 respectively corresponding to x_{obs} and x_{mod} in Equation (1.1). The x_{mod} considered
153 is the ERA5-Land dataset (Muñoz-Sabater et al., 2021), while x_{obs} is the Coperni-
154 cus regional reanalysis for Europe (CERRA-Land) dataset (Verrelle et al., 2021)
155 (ECMWF reanalysis can be freely downloaded through the Climate Data Store).
156 Both datasets cover Europe on a large range of climate variables and are produced by
157 the European Centre for Medium-Range Weather Forecast (ECMWF). The ERA5-L
158 reanalysis is a global reanalysis with a $0.1^\circ \times 0.1^\circ$ (approx. 11×11 km) resolution,
159 spanning from 1950 to 2021, while the CERRA-L database is a high-resolution
160 reanalysis at 5.5×5.5 km resolution from January 1984 to July 2021. In this study,
161 we considered 36 common years from 01/01/1985 to 31/12/2020. The CERRA-L
162 uses the ERA5 (C3S, 2018) reanalysis for assimilation while ERA5-L is a spatially
163 enhanced version of ERA5 over the dry land areas. The CERRA-L data being on
164 a regular kilometres grid has been interpolated to a regular longitude-latitude grid
165 using the linear scattered interpolant (`scatteredInterpolant`) from MATLAB (The
166 MathWorks Inc., 2022). Then, the ERA5-L data has been interpolated to the same
167 grid as a simple mapping step using Python’s library `SciPy CloughTocher2D` inter-
168 polator. While the ERA5-L reanalysis has been extensively used for climate studies
169 (Yang et al., 2023; Malaekheh et al., 2022), the CERRA-L dataset is still new and has
170 not seen many published studies based on its data (Monteiro and Morin, 2023), and
171 none, to the best of our knowledge, for precipitation modelling and bias correction. A
172 visual analysis at the median and 99.5th quantile of daily precipitation over the con-
173 sidered period shows the similarity as well as the differences between both reanalysis
174 when it comes to daily rainfall.

175

176 Figure 1 (a,b) clearly shows similar median precipitations over France with differences
177 mainly focused on high-altitude areas (Massif Central and Alps region). While most
178 of France has a daily median precipitation of around 3 to 5mm per day, the Massif
179 Central region receives close to 10mm of precipitation for CERRA-L shown in Figure
180 1 (a), but only 7mm for ERA5-L in (b). These differences are much more noticeable
181 when looking at the extremes in the Cévennes region reaching 160mm for CERRA-
182 L in Figure 1 (c,d), while the same region does not exceed 100mm for ERA5-L. The
183 impact of higher resolution over strong orography regions is clear for extreme daily
184

precipitations. Values from ERA5-L are smoothed compared to CERRA-L and interpolating the data to a higher resolved grid cannot bring relevant variability, thus the clear need for bias correction.

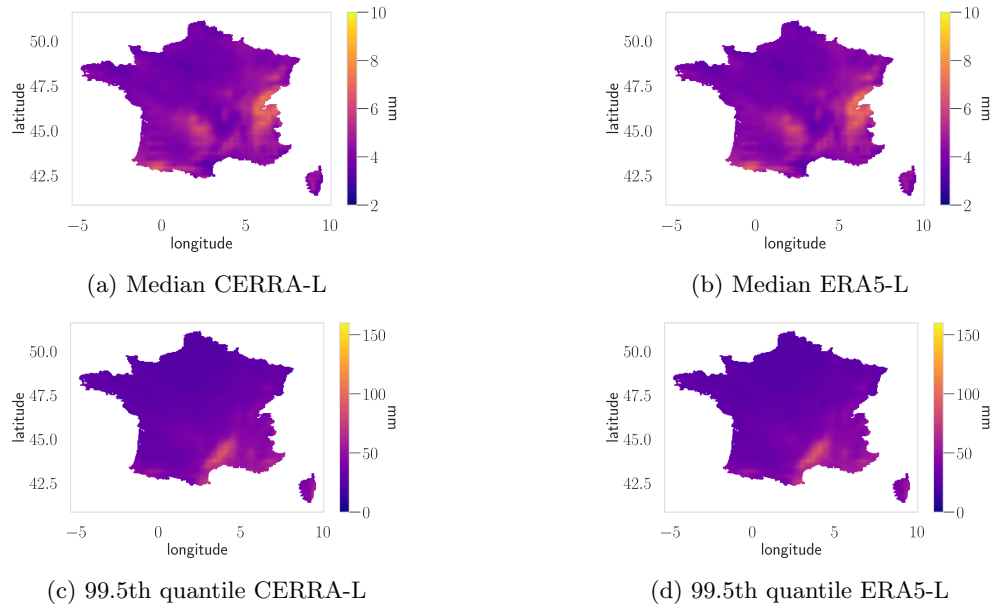


Fig. 1: Median (panels a and b) and 99.5th quantile (panels c and d) daily precipitation in mm over the considered period for CERRA-L reanalysis data (first column) and ERA5-L reanalysis data (second column)

In this paper, we only consider wet days of the given time series, with a threshold for wet days at 1 mm. This means no correction over the dry days' proportion is done and the corrected data will keep the same number of dry and wet days. The number of wet days differs from point to point, but the range is from 2627 to 7274 days for ERA5-L and 1759 to 7641 days for CERRA-L (for a total of 13149 days).

Since both reanalysis were produced from the ECMWF and are influenced by a common reanalysis ERA5, a first naive approach could be to avoid the bias correction phase, *i.e.*, not apply Equation (1.1). However, this would result in erroneous models and impact studies. To illustrate this error, the Mean Absolute Error (MAE) and Mean Absolute Error over the 95th quantile (MAE95sup) metrics (see Appendix A for details) have been computed without any bias correction (see Figure 2).

185
186
187
188
189
190
191
192
193
194
195
196
197
198
199
200
201
202
203
204
205
206
207
208
209
210
211
212
213
214
215
216
217
218
219
220
221
222
223
224
225
226
227
228
229
230

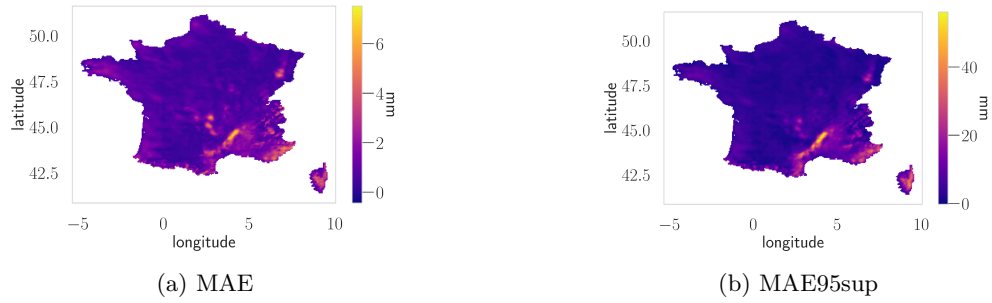


Fig. 2: Error metrics in mm (see Appendix A) between the CERRA-L and ERA5-L reanalysis without bias correction

Both maps in Figure 2 show significant bias in the uncorrected interpolated ERA5-L reanalysis. The median MAE is around 0.60mm with peaks at 7.02mm while the median MAE95sup is at 3.43mm with peaks at 55.61mm.

Then, bias correction in Equation (1.1) seems to be a necessary step to correctly use those datasets in the impact studies. Based on this consideration, we now aim to build a flexible distributional model to fit both reanalysis precipitation datasets to apply Equation (1.1). This is the goal of the next section.

2 The proposed semi-parametric stitch distributional model

2.1 An adapted goodness-of-fit statistical test

The well-known Kolmogorov-Smirnov (KS) (Massey Jr., 1951), Cramer-von Mises (CvM) (Anderson, 1962) and the Anderson-Darling (AD) (Anderson and Darling, 1954) are the most commonly used statistical tests to evaluate the adequacy of a distribution and eventually discriminate between multiple models (Laio, 2004; Vlček and Huth, 2009). However, the KS and CvM tests tend to underestimate the deviation that occurs in the tail of the distribution (Steinskog et al., 2007) and while the AD test includes a weight function able to increase the sensitivity on the distribution tails and standardizes the variance, the AD test still mishandles the tails (Moscovich et al., 2016). Instead of looking at the deviations of the distributions, the Berk-Jones (BJ) statistical test (Berk and Jones, 1979) uses the most statistically significant deviation. In this paper, we will use an adapted version of the consistent BJ test to determine the best-fitting models for a considered time series. Let us introduce some notations:

- Let $\tilde{x} := \{\tilde{x}_1, \dots, \tilde{x}_n\}$ be an *i.i.d* sample from a random variable X . Let X follow a continuous cumulative distribution function (cdf) F . Then, under the null hypothesis $\mathcal{H}_0 : X \sim F$. The alternative hypothesis will be $\mathcal{H}_1 : X \not\sim F$.
- Let $x := \{x_{(1)}, \dots, x_{(n)}\}$ be empirical quantiles of the sample \tilde{x} , with $x_{(1)} < x_{(2)} < \dots < x_{(n)}$ which are the order statistics of x (we can safely assume that none of the *i.i.d* samples are equal).

- We also denote the quantile of a distribution F corresponding to the i -th ordered quantile as $F^{-1}(\frac{i-1}{n}) = q_{(i),F}$, with F the candidate distribution fitted on x . Let $q := \{q_{(1),F}, \dots, q_{(n),F}\}$.

The random variable $F(X)$ follows a uniform distribution $U[0, 1]$ by the probability integral transform result. Let consider $u_{i,F} = F(x_{(i)})$ for $i = 1, \dots, n$ an *i.i.d* sample from the $U[0, 1]$ distribution and the corresponding order statistics $u_{i,F}$. We know that under \mathcal{H}_0 , $u_{i,F}$ is a random sample from u_i which has a known distribution:

$$u_i \sim \text{Beta}(i, n - i + 1), \quad \text{for } i = 1, \dots, n. \quad (2.1)$$

The BJ test then computes the following p -values:

$$p_{i,F}^* := \mathbb{P}(\text{Beta}(i, n - i + 1) < u_{i,F}). \quad (2.2)$$

For each i , we can then define:

$$p_{i,F} = \min(p_{i,F}^*, 1 - p_{i,F}^*). \quad (2.3)$$

In [Moscovich and Nadler \(2017\)](#), the M_n statistic is defined by:

$$M_n := \min_{1 \leq i \leq n} p_{i,F} \in [0, 1], \quad (2.4)$$

where small values of M_n describe a bad fit of the candidate distribution F . The p -value associated to α , denoted $p_{\alpha,n}$, is given by $\mathbb{P}(M_n \leq p_{\alpha,n}) = \alpha$. Theoretical properties including the asymptotic consistency of the BJ statistics and algorithms to explicitly compute the p -values in Equation (2.3) can be found in [Moscovich et al. \(2016\)](#); [Moscovich and Nadler \(2017\)](#); [Moscovich \(2023\)](#).

The BJ statistical test can detect deviations in both tails of the distributions. In the case of skewed distributions, such as the ones used for precipitation modelling, most of the weight is concentrated in the lower tail, making it harder to detect deviation from the upper tail. However, heavy upper tail behaviour is a crucial issue if one aims to model extremely large precipitation events. The way the BJ test is constructed allows to associate each quantile (or rank) with a p -value. We can then use this p -value to determine if the considered quantile deviation would have been enough to give a rejection or not.

In practice, this translates to not severe enough statistics produced by the extreme deviations, and errors of 50mm or even 150mm may not be considered significant enough by the statistical test. Indeed the rejection threshold for such events, even for $\alpha = 15\%$ may be 10 or 20 times lower than the associated $p_{i,F}$ in Equation (2.3). To increase the severity of the BJ test on the upper tails, we introduce a weight using the prediction error between $x_{(i)}$, the ordered statistic of rank i , and the modelled

323 corresponding quantile from the candidate distribution $q_{(i),F}$. We define the *weighted-*
324 *level* $k_{i,F}$ such that

$$325 \\ 326 k_{i,F} := \frac{p_{i,F}}{\max(|x_{(i)} - q_{(i),F}|, 1)}, \quad \text{for } i = 1, \dots, n. \quad (2.5) \\ 327$$

328 The $p_{i,F}$ assesses the goodness of fit for the rank i . The same consideration could
329 be applied on the weighted-level $k_{i,F}$ in (2.5) on the extremely large precipitation
330 quantile levels. For daily precipitation data, a high prediction error will typically be
331 magnitudes greater than 1mm. Thus, in these cases, the weighted-level as defined in
332 Equation (2.5) will be greatly reduced compared to the corresponding $p_{i,F}$, making it
333 much easier to detect. The weighted-levels are penalizing large deviations in the tails
334 by reducing the corresponding $p_{i,F}$. Such deviations should mostly occur when \mathcal{H}_0 is
335 **False**, especially for large enough sample sizes. While no theoretical proof is given
336 for the guarantee of the test significance level or power, one can conjecture that this
337 modification increases the power of the test.
338

339 2.2 Cutting indexes for the semi-parametric model

341 Sometimes, a single parametric distribution is not flexible enough to describe daily
342 rainfall time series on a broad range of locations. The selected model may only be
343 adequate up to (or starting from) a specific quantile and be misfitted otherwise.
344 To overcome this, we introduce a semi-parametric distribution based on the modified
345 BJ test introduced in Section 2.1 and on three distinct distribution types:

- 347 • A main heavy-tailed distribution F_{heavy} ,
- 348 • A secondary lighter-tailed distribution $F_{lighter}$,
- 349 • The empirical distribution of the data F_n .

350 The idea is quite simple: replace the badly fitted portion of the heavy-tailed distri-
351 bution with the lighter-tailed distribution using the previously adapted BJ test, and
352 finally, if needed, replace the upper and lower tails with the empirical distribution.
353 Precipitation modelling via semi-parametric distributions has been explored by a
354 few authors. The most common version is a stitch between a first distribution mod-
355 elling low and moderate precipitations and a Generalized Pareto distribution for the
356 extremes, also known as spliced distribution (Li et al., 2012; Castro-Camilo et al., 2019;
357 Kim et al., 2019). The main issue with semi-parametric and hybrid distribution is the
358 difficult selection of an appropriate threshold. This latter needs to be high enough in
359 the case of the Generalized Pareto so the Pickands–Balkema–de Haan theorem can be
360 applied (see Pickands (1975) and Balkema and Haan (1974)).

361 To implement our stitch model, we introduce the cutting indexes for a distribution F
362 from the p -values and weighted values $p_{i,F}$ and $k_{i,F}$ from Equations (2.3) and (2.5),
363 as follows.
364

365 **Definition 1 (Cutting indexes).** *Let $x_{(i)}$ and $q_{(i)}$ be respectively the empirical and*
366 *modelled quantiles from a time series as described in Section 2.1. Let $p_{i,F}$ and $k_{i,F}$ be*
367 *the p -values and weighted levels induced from the BJ test as in Equations (2.3) and*
368

(2.5). Let $p_{\alpha,n}$ be the rejection threshold at level α for the BJ test for a sample size n , i.e., such that $\mathbb{P}(M_n \leq p_{\alpha,n}) = \alpha$. Let \mathbf{lag} be a strictly positive natural number.

1. **Lower cutting index.** The lower tail is considered adequate if and only if there are no rejections at level $p_{\alpha,n}$ for the next \mathbf{lag} indexes. We define the lower cutting index $i_{\ell,F}$ as equal to 0 if no rejection is detected at level $p_{\alpha,n}$ for the first \mathbf{lag} ordered quantiles. Conversely, if a rejection is detected, we consider the first rank not rejected at level $p_{\alpha,n}$, such that the next \mathbf{lag} p -values are also not rejected at the same level. Formally we can write

$$i_{\ell,F} = i - 1 \begin{cases} \forall 0 \leq j < i, \exists 0 \leq k \leq \mathbf{lag}, p_{(j+k),F} < p_{\alpha,n}, \text{ and} \\ \forall 0 \leq j \leq \mathbf{lag}, p_{(i+j),F} \geq p_{\alpha,n}. \end{cases} \quad (2.6)$$

2. **Upper cutting index** The upper tail is considered adequate if and only if there are no rejections at $p_{\alpha,n}$ for the previous \mathbf{lag} indexes. More precisely, we define the upper cutting index $i_{u,F}$, as the first index $n - i - 1$, for $0 \leq i < n$, satisfying the following two conditions: the corresponding weighted level is not rejected at $p_{\alpha,n}$ and the previous \mathbf{lag} weighted levels are also not rejected at $p_{\alpha,n}$.

$$i_{u,F} = n - i - 1 \begin{cases} \forall i < j \leq n, \exists 0 \leq k \leq \mathbf{lag}, p_{(j-k),F} < p_{\alpha,n} \text{ and} \\ \forall 0 \leq j \leq \mathbf{lag}, k_{(n-i-j),F} \geq p_{\alpha,n}. \end{cases} \quad (2.7)$$

Notice that $i_{u,F}$ can be equal to $n - 1$ (resp. $i_{\ell,F}$ can be equal to 0), which indicates that no cut in the upper (resp. lower) tail of the considered distribution is needed. From the upper and lower cutting indexes defined in Definition 1 (see Equations (2.6) and (2.7)), we can list five types of possible rejections, denoted $\mathbf{typeRej}_F$ in the following.

Definition 2 (Types of rejection).

$\mathbf{typeRej}_F == 1$ No rejection: $i_{\ell,F} = 0$ and $i_{u,F} = n - 1$, neither the lower nor the upper tail have been cut and the distribution F is kept as initially fitted.

$\mathbf{typeRej}_F == 2$ Left rejection: $i_{\ell,F} > 0$, only the lower tail of the distribution has been rejected at some degree and will be replaced.

$\mathbf{typeRej}_F == 3$ Right rejection: $i_{u,F} < n - 1$, only the upper tail of the distribution has been rejected at some degree and will be replaced.

$\mathbf{typeRej}_F == 4$ Double rejection: $i_{\ell,F} > 0$ and $i_{u,F} < n - 1$, both a left and right rejection occurs and the distribution will be replaced for both tails.

$\mathbf{typeRej}_F == 5$ Total rejection: If the rejection on the upper tail or the lower tail is too strong, we decide to completely reject the distribution. In particular for the upper tail: if $i_{u,F} < l_{upper}$, the whole distribution is rejected. For the lower tail: if $i_{\ell,F} > l_{lower}$ and at least one point is rejected in the upper tail ($i_{u,F} < n - 1$), the whole distribution is rejected.

In the previous Definitions 1 and 2, \mathbf{lag} , l_{upper} and l_{lower} are all hyperparameters to be calibrated. In our procedure, we evaluate $i_{\ell,F}$ and $i_{u,F}$ in Equations (2.6)-(2.7) and

415 the rejection types typeRej_F in Definition 2 with F being either F_{heavy} or $F_{lighter}$.
 416 Secondly, three booleans variables are defined as follows.

417

418 **Definition 3 (Rejection booleans).** *Let us define r_{right} as a boolean variable which*
 419 *will be **True** if we replaced the upper tail of F_{heavy} with the upper tail of $F_{lighter}$ (a*
 420 *lighter-tailed distribution). Then*

421

$$422 \quad r_{right} = (\text{typeRej}_{F_{lighter}} == 1 \text{ or } \text{typeRej}_{F_{lighter}} == 2) \text{ and } \text{typeRej}_{F_{heavy}} \geq 3$$

423

424 *In this situation, the last $i_{u,F_{heavy}}$ of F_{heavy} quantiles will be replaced with the $F_{lighter}$'s*
 425 *ones.*

426 *Let us define r_{left} as a boolean variable which will be **True** if $F_{lighter}$ replaces F_{heavy} 's*
 427 *lower tail. Then*

428

$$429 \quad r_{left} = \begin{cases} (\text{typeRej}_{F_{lighter}} == 1 \text{ or } \text{typeRej}_{F_{lighter}} == 3) & \text{and} \\ (\text{typeRej}_{F_{heavy}} == 2 \text{ or } \text{typeRej}_{F_{heavy}} == 4) \end{cases}$$

430

431 *In this case, the $i_{l,F_{heavy}}$ first quantiles of F_{heavy} will be replaced by the corresponding*
 432 *quantiles of $F_{lighter}$.*

433 *Let us define r_{all} as a boolean variable which will be **True** if $F_{lighter}$ completely replaces*
 434 *F_{heavy} . Then*

435

$$436 \quad r_{all} = \begin{cases} \text{typeRej}_{F_{lighter}} == 1 \text{ and } \text{typeRej}_{F_{heavy}} == 4 & \text{or} \\ \text{typeRej}_{F_{lighter}} \leq 4 \text{ and } \text{typeRej}_{F_{heavy}} == 5 \end{cases}$$

437

438 *In this case, $F_{lighter}$'s quantiles will completely replace F_{heavy} 's quantiles.*

439 The resulting model will be called below the Semi-Parametric Stitch Berk-Jones based
 440 model (Stitch-BJ model or Stitch-BJ distribution in the rest of this paper).

441 Combining two distribution functions or stitching their quantile functions should be
 442 done carefully to preserve classical properties. An analytical version of the resulting
 443 distribution can be found in Appendix C as well as a proposed process to guarantee
 444 the monotonicity of the resulting quantile function.

445

446 In the next section, we apply the proposed stitch semi-parametric distributional model
 447 to the ERA5-L and CERRA-L reanalysis datasets.

448

449 3 Stitch-BJ model on reanalysis over France

450

451 We chose here (see Appendix B for details):

452

- 453 • F_{heavy} = Extended Generalized Pareto distribution (EGPD),
- 454 • $F_{lighter}$ = Exponentiated Weibull distribution (ExpWD),

455

456 The EGPD is supposed to be able to model both light and heavy-tailed data (Naveau
 457 et al., 2016). The ExpWD is an extension of the Weibull distribution and has been
 458 chosen for its ability to be both light or heavy-tailed depending on its shape parameter.

459

Moreover, when its shape parameter is equal to 1, the ExpWD becomes a special case of the EGPD. 461

When taking the quantile at level 1 of parametric distributions, we actually take the quantile $1 - \frac{1}{n+1}$ with n the number of wet days for the selected location. 462

Hyperparameters values in Definition 2 are fixed in our case study, both for ERA5-L and CERRA-L, as follows: 463

$$l_{upper} = \lfloor 97\% \times n \rfloor, l_{lower} = \lfloor 50\% \times n \rfloor \text{ and } lag = \lfloor 1\% \times n \rfloor, 464$$

where $\lfloor \cdot \rfloor$ is the floor number operator and n is the number of wet days of the given time series. The l_{upper} and l_{lower} hyperparameters are quite stable for our study, with results being similar when small changes were applied to these parameters. The lag parameter allows to adjust the sensitivity of the detection: a high value will make the detection very sensitive to rejections, since a lone rejection happening far from a tail may cause the whole tail to be rejected. This last parameter has been chosen based on trials not shown here. 465

Applications 1, 2 and 3 below describe the steps we implemented to obtain a Stitch-BJ model for the ERA5-L and CERRA-L reanalysis. 466

Application 1 Rejections type and cutting indexes for the EGPD 467

Step (1) Let us consider x and q_{EGP} (see Section 1.2) the empirical quantiles and the EGPD quantiles for a reanalysis data in a specific grid point of the French territory. 468

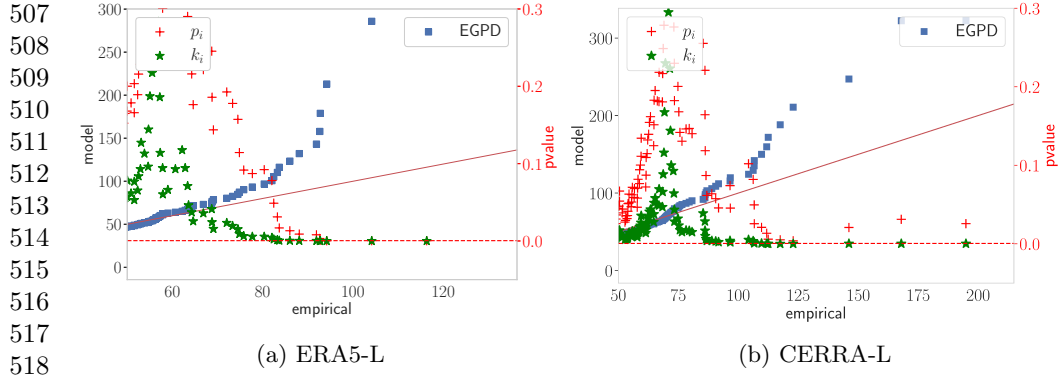
Step (2) From Equations (2.2)-(2.3), compute $p_{i,EGP}^*$ and $p_{i,EGP}$, for the considered EGPD in Step (1). 469

Step (3) Compute the weighted-levels $k_{EGP} = \{k_{i,EGP}, i = 1, \dots, n\}$ as in Equation (2.5). 470

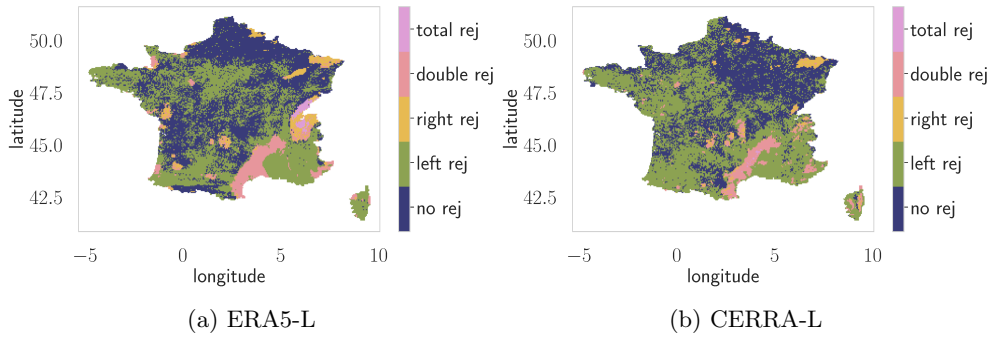
Step (4) Compute the cutting indexes and type of rejection $i_{\ell,EGP}, i_{u,EGP}$ and typeRej_{EGP} as described in Definitions 1 and 2. 471

Steps (2) and (3) of Application 1 with respect to the empirical quantiles x are illustrated in Figure 3. On both panels of Figure 3, the impact of the weighted-levels $k_{i,EGP}$ in Equation (2.5) on the upper tail is noticeable. For panel (a), the $k_{i,EGP}$ are rejected much faster than the original p -values $p_{i,EGP}$, allowing the model to detect misfitted quantiles better. On panel (b), the impact is even more noticeable with the original $p_{i,EGP}$ never crossing the rejection threshold $p_{\alpha,n}$ for the upper tail, while the fit error exceeds 100m for some quantile points. 472

On both panels of Figure 4, one can appreciate that the vast majority of locations in the considered French territory are either fully accepted (no rejection) or rejected only on the lower tail (left rejection). Some regions exhibit fit that is not satisfying enough with a high density of rejection of type 4 and 5 (respectively corresponding to a rejection of both tails and a total rejection). Those regions are mainly focused around the Cévennes and Alps regions for the ERA5-L reanalysis and the Cévennes 473



519 **Fig. 3:** Blue squares: Quantile-quantile plot of the EGP model at location (Longitude
520 2.94, Latitude 42.53). Red crosses: $p_{i,EGP}$; green stars: $k_{i,EGP}$, for $i = 1, \dots, n$. The
521 horizontal red dashed line is the rejection threshold $p_{\alpha,n}$, for $\alpha = 5\%$. The scale for
522 $p_{i,EGP}$ and $k_{i,EGP}$ is represented in red on the right side
523



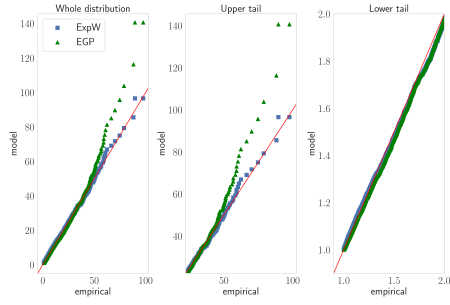
536 **Fig. 4:** Rejection type map for the EGPD over France using $\alpha = 5\%$ for our two
537 reanalysis datasets.
538

539
540 region for the CERRA-L reanalysis. To improve the model on these locations, we
541 replace the misfitted portions of the EGPD with the ExpWD (see Appendix B for
542 details) as described in Application 2 below.
543

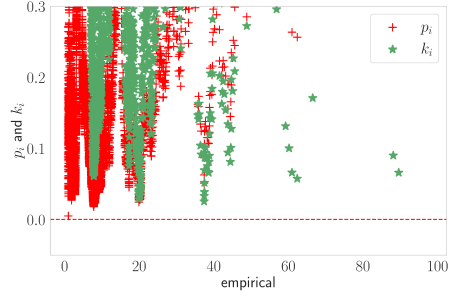
544 QQ-plots in Figure 5 (panels a and c) show the difference for two chosen locations
545 between the modelled EGP quantiles and the ExpW ones in ERA5-L (panel a) and
546 CERRA-L (panel c) data. Here we decided to replace the upper tail of the EGP
547 with the ExpW one, due to the high errors of the last EGP quantiles. This can specifically
548 be seen on panel (c) where the last quantiles have a fit error of almost 200mm. To
549 illustrate Application 2, in Figure 5 (panels b and d) we also display the correspond-
550 ing $p_{i,ExpW}$ (red crosses) and $k_{i,ExpW}$ (green stars) in Equations (2.3) and (2.5).
551 Notice that all $k_{i,ExpW}$ are larger than $p_{\alpha,n}$, meaning that the ExpW upper tail is
552

Application 2 Exponentiated Weibull distribution replacement	553
Step (1) Compute $p_{ExpW}, k_{ExpW}, i_{\ell,ExpW}, i_{u,ExpW}$ and typeRej_{ExpW} as in Application 1 (Step 2 to 4), for the ExpW distribution. Set the boolean variables $r_{\text{right}}, r_{\text{left}}$ and r_{all} as in Definition 3.	554
Step (2) If r_{right} is True , replace the last $n - 1 - i_{u,EGP}$ quantiles by the corresponding ExpW quantiles.	555
Step (3) If r_{left} is True , replace the first $i_{\ell,EGP}$ quantiles by the corresponding ExpW quantiles.	556
Step (4) If r_{all} is True , replace totally by the ExpW distribution.	557
	558
	559
	560
	561
	562
	563
not rejected and will replace the EGP upper tail for these locations.	564
	565
While most locations can be modelled via Application 2 using only parametric distributions (see for instance locations in Figure 5), for some locations with complex and particularly skewed distributions, we chose to use the empirical distribution to replace the misfitted parts, as detailed in Application 3 below.	566
	567
	568
	569
	570
	571
Application 3 Empirical distribution replacement	572
Step (1) If r_{left} is False and $i_{\ell,EGP} > 0$, replace the first $i_{\ell,EGP}$ quantiles by the empirical ones.	573
Step (2) If r_{right} is False and $i_{u,EGP} < (n - 1)$, replace the last $n - i_{u,EGP} - 1$ quantiles by the empirical ones.	574
Step (3) If r_{all} is False and $\text{typeRej}_{EGP} == 5$, replace totally by the empirical distribution.	575
Step (4) If r_{all} is True and $i_{\ell,ExpW} > 0$, replace the first $i_{\ell,ExpW}$ quantiles by the empirical ones.	576
Step (5) If r_{all} is True and $i_{u,ExpW} < (n - 1)$, replace the last $n - i_{u,ExpW} - 1$ quantiles by the empirical ones.	577
	578
	579
	580
	581
	582
	583
	584
In Figure 6, neither the EGP nor the ExpW distribution seems to be able to model the upper tail and the lower tail correctly. In this case, the empirical distribution will be used to model both tails on this specific location. Indeed both the ExpW and EGP distributions meet the conditions for a double rejection as defined in Definition 2. In Figure 6 we show the lower and upper index $i_{\ell,EGP}$ and $i_{u,EGP}$. By using Application 3, the final stitch model with the lower and upper tails replaced by the empirical distribution is called Replaced in Figure 6 (red triangles).	585
Moreover, Figure 6 illustrates cases where the monotonicity of the resulting final quantile function may be broken. For instance here, at $i_{u,EGP}$, the last EGP quantile used is at around 180mm while the next quantile taken from the empirical distribution is at around 110mm (see Figure 6 panel b, upper tail QQ-plot). A break in monotonicity can also be detected on the lower tail at the $i_{\ell,EGP}$ cutting point (see Figure 6 panel b, lower tail QQ-plot). We propose a simple method to correct breaks	586
	587
	588
	589
	590
	591
	592
	593
	594
	595
	596
	597
	598
	599

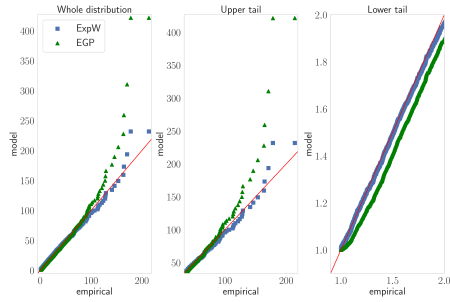
599
600
601
602
603
604
605
606
607
608
609
610
611
612
613
614
615
616
617
618
619
620
621
622
623
624
625
626
627
628
629
630
631
632
633
634
635
636
637
638
639
640
641
642
643
644



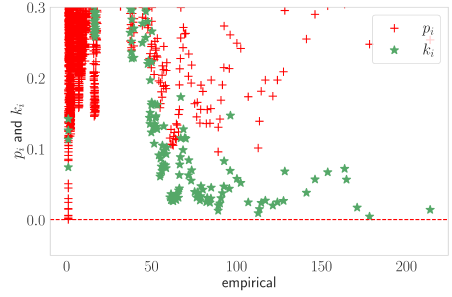
(a) ERA5-L at (Longitude 6.89, Latitude 44.86)



(b) ERA5-L at (Longitude 6.89, Latitude 44.86)



(c) CERRA-L at (Longitude 9.42, Latitude 42.53)

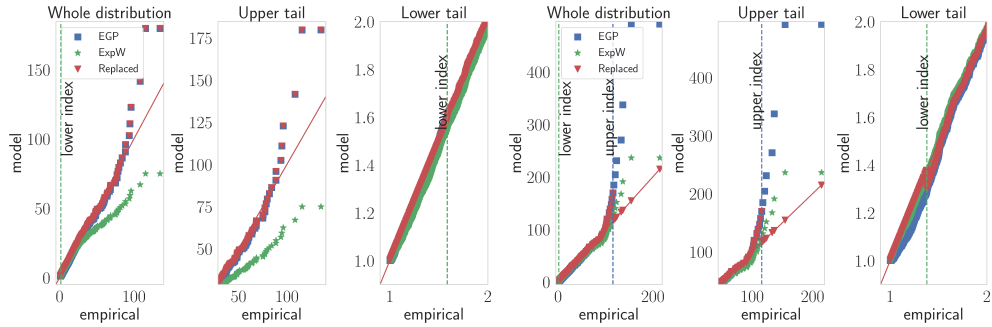


(d) CERRA-L at (Longitude 9.42, Latitude 42.53)

Fig. 5: First row: ERA5-L location. Second row: CERRA-L location. First column: QQ-plot of respectively the whole, upper (above 97th quantile) and lower tail of the EGP (green triangles) and ExpW (blue squares) against the empirical data. Second column: corresponding $p_{i,ExpW}$ (red crosses) and $k_{i,ExpW}$ (green stars). Red horizontal line is the rejection threshold $p_{\alpha,n}$ for $\alpha = 5\%$

in the monotonicity, which is presented in Appendix C.

Figure 7 shows the final and detailed stitch combination using Applications 1, 2 and 3, on every location for ERA5-L and CERRA-L reanalysis dataset.



(a) ERA5-L at (Longitude 9.18, Latitude 42.39) (b) CERRA-L at (Longitude 2.61, Latitude 42.67)

Fig. 6: QQ-plot of the EGP model (blue square), ExpW model (green stars) and the EGP with empirical stitching model (red triangle). Green (resp. blue) dashed line is the lower (resp. upper) cutting index $i_{l,EGP}$ (resp. $i_{u,EGP}$) as in Definition 1 for the EGP model.

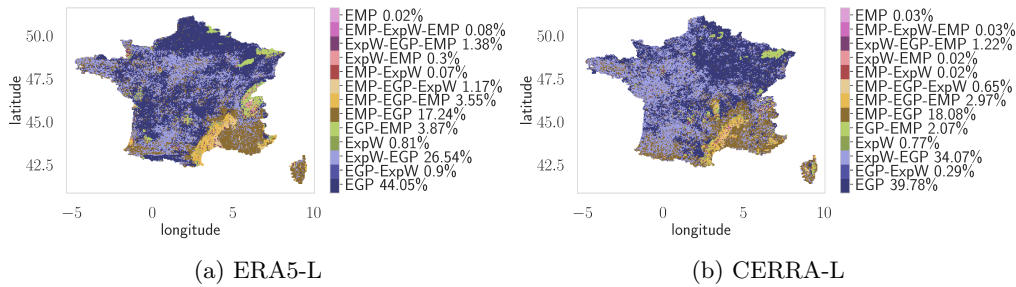


Fig. 7: Final map of the Stitch-BJ model with the EGP (EGPD) and ExpW (WEIB) and empirical (EMP) distributions. We display the proportion of locations for each combination of models for both considered datasets

For both reanalyses, we can see that the vast majority of points are modelled using fully parametric distributions, either with no modification or using a stitch. Interestingly, for ERA5-L and CERRA-L datasets, a few locations (respectively less than 9% and 6.3%) use the empirical distribution to correct the upper tail and less than respectively 0.02% and 0.03% use the empirical distribution to fully model the location's precipitation distribution. For almost 75% of the locations, a full parametric distribution has been used for both datasets.

A more precise description of the number of locations where the lower (resp. upper) tail has been replaced by an empirical (resp. parametric) distribution is available in Table 1. Note that the proportion of lower and upper tail replacement locations

Table 1: Summary of empirical and parametric distributions used for the Stitch-BJ over France

EMPIRICAL				
	LOWER TAIL	UPPER TAIL	BOTH TAILS	FULL
ERA5-L	18.48 %	5.56 %	3.63 %	0.02 %
CERRA-L	18.75 %	3.31 %	3.00 %	0.03 %
PARAMETRIC				
	LOWER TAIL	UPPER TAIL	BOTH TAILS	FULL
ERA5-L	5.56 %	18.48 %	0 %	72.30 %
CERRA-L	3.31 %	18.75 %	0 %	74.91 %

by the empirical or parametric distributions only concern *strictly lower or upper replacements*. If a location has been replaced on both tails or fully by the empirical distribution, it is not taken into account in the lower and upper tail replacement proportion. This explains why one needs to add the proportion of lower tail and upper tail replacement of either the parametric or empirical distribution to the proportion of both tail replacement and total replacement of both types of distributions to reach 100%. To complete the information provided in Table 1, the distributions (via boxplots) of the cutting indexes are available in Appendix D.

In the next section, we discuss the results of the proposed fitting procedure (Applications 1, 2 and 3) on both datasets (see Section 4.2). Then we use it in a bias correction context (see Section 4.3).

4 Results

In this section, we evaluate the fit and the bias correction performance of the proposed Stitch-BJ and we compare it with several classical parametric competitors. For the fitting results (see Section 4.2), distributions are fitted to the wet days time series separately for ERA5-L and CERRA-L data. For the bias correction results (see Section 4.3), we use both ERA5-L and CERRA-L fitted distributions to bias correct ERA5-L time series. Note that the distributions are fitted on the whole period (01/01/1984-31/12/2020) for both datasets as a simple application of a bias correction using the quantile mapping method.

Using Equation (1.1), we identify:

- $F_{n,obs}^{-1}$ is the quantile function of the considered distribution fitted on CERRA-L.
- $F_{n,mod}$ is the cdf of the considered distribution fitted on ERA5-L
- x_{mod} is a wet-day time series of ERA5-L.

After bias correction in (1.1), quantiles of x_{mod}^{corr} (the bias-corrected time series) are compared to the quantiles of x_{obs} (the corresponding wet-days time series from CERRA-L).

4.1 Instructions for figures interpretation	737
In the following, multiple figures illustrate the performance of the proposed method (for fit and bias correction) compared with more classical parametric distributions. Four types of figures are shown:	738
1. Error maps for a specific metric for considered models.	739
2. Error differences maps between the proposed method and considered models for a specific metric.	740
3. Error boxplots for the considered models for a specific metric.	741
4. QQ-plots for some selected locations.	742
Type 1 Figures 8, 9, 14, 15, 21 and 22 are the error maps for a given metric. The error is evaluated between the empirical and the fitted quantiles for the fit section, and between the corrected ERA5-L and CERRA-L quantiles for the bias correction section. We limited the values range to reach the 99.9th quantile of the error produced by our Stitch-BJ model for comparison.	743
	744
	745
	746
	747
Type 2 Figures 10, 11, 16, 17, 23 and 24 show the differences between the Stitch-BJ and the other distributions for a given metric. Contrary to Type 1 figures, the error range is not fixed and differs for each sub-figure, thus covering the whole range of error differences for each distribution. Here, a positive (resp. negative) value indicates that the competitor distribution performs better (resp. worst) than the Stitch-BJ one. Note that the error range is not symmetric.	748
	749
	750
	751
	752
	753
	754
	755
	756
	757
	758
	759
	760
Type 3 Figures 12, 13, 18, 19, 25 and 26 are boxplots of Type 1 figure results. To show both the lower and the extreme errors, a jump in the y-axis is implemented. The horizontal dashed line represents the median error for the Stitch-BJ method. A second boxplot, without the jump but zoomed on the median values is also shown. The upper limit of the zoomed boxplot corresponds to the 3rd quartile of the worst distribution for the considered boxplot.	761
	762
	763
	764
	765
	766
	767
Type 4 Figure 20 are QQ-plots of some selected locations, showing the quantile-per-quantile performance of each method compared to the ground truth. For all Type 4 figures, blue squares represent time series modelled from the Stitch-BJ method, the orange triangles from the EGPD and green crosses from the ExpWD. The red line corresponds to the empirical quantile line. For the fit results, Type 4 figures also include a short description of the resulting Stitch-BJ model by giving the selected distributions of the proposed stitch. For example: EMP-EGP-ExpW means the lower tail uses the empirical distribution, the centre is modelled by the EGPD and the upper tail uses the ExpWD.	768
	769
	770
	771
	772
	773
	774
	775
	776
	777
4.2 Fit results	778
As explained previously, bias correction requires the same distribution to be fitted twice: once on the starting, biased data (ERA5-L), and once on the target data (CERRA-L). While the two reanalyses show some similarities, differences between the	779
	780
	781
	782

783 resulting fitting procedure described in Section 3 are expected. We will study the fit
 784 for the Stitch-BJ, EGP, ExpW and Gamma distributions globally over France, and
 785 provide a local analysis into some selected locations.

786 Both datasets used a daily 1mm threshold to remove the drizzle effect (Chen et al.,
 787 2021) and distributions are solely fitted on wet days precipitations. A location param-
 788 eter was available for all distributions except the EGPD. A left shift of 1mm has been
 789 applied when fitting to the EGPD (and constructing the Stitch-BJ) to compensate
 790 for that. The shift is reintroduced when the quantile function of these distributions is
 791 used. For the EGPD, a 3mm left censor has been used. This value was chosen after
 792 testing and resulted in the best performance for our application. The interested reader
 793 is also referred to Appendix B for details.

794

795 4.2.1 Spatialized metrics

796

797 Figures 8 and 9 display the MAE maps (see Appendix A) for the distributions fitted
 798 on respectively ERA5-L and CERRA-L.

799

800

801

802

803

804

805

806

807

808

809

810

811

812

813

814

815

816

817

818

819

820

821

822

823

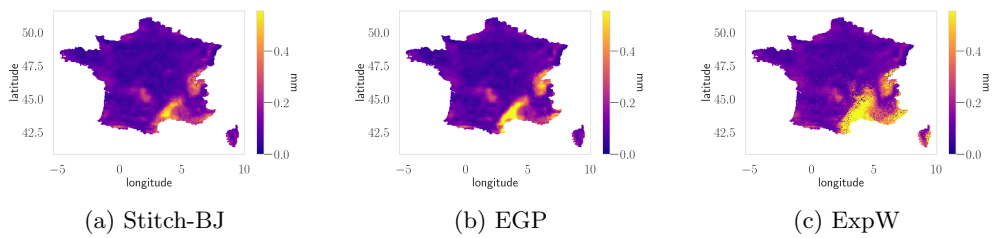
824

825

826

827

828



808 **Fig. 8:** MAE of considered models fitted to ERA5-L over Metropolitan France

810

811

812

813

814

815

816

817

818

819

820

821

822

823

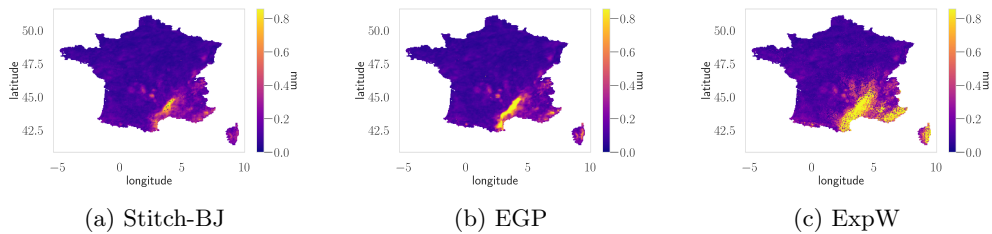
824

825

826

827

828



820 **Fig. 9:** MAE of considered models fitted to CERRA-L over Metropolitan France

823 For the ExpW model, the errors' spatial distribution is quite similar to the EGP one,
 824 with high errors being more prominent in the Cévennes and around the city of Nice.
 825 The Stitch-BJ shows differences mainly focused around the Cévennes and Alps region
 826 where it has an improvement with very few locations exceeding the 0.5mm MAE for
 827 ERA5-L (Figure 8) and 0.8mm for CERRA-L (Figure 9). Notice that most of the

Cévennes region exceeds this threshold for the EGPD and ExpWD. The Gamma distribution map is not shown as its errors are very large over most of France (see boxplots in Figures 12 and 13).

By analysing the differences maps in Figures 10 and 11, the EGPD seems to perform better than the Stitch-BJD in specific locations, but when looking carefully at the actual improvement, the MAE is only slightly reduced. Conversely, the improvements of the Stitch-BJD over both the EGPD and ExpWD (in particular around the Cévennes region) are important in magnitude.

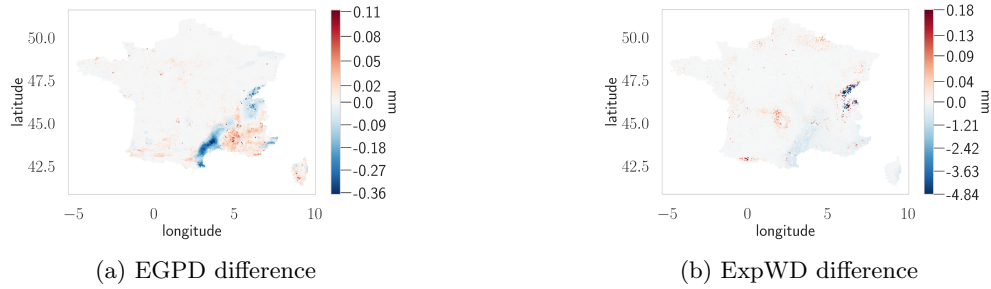


Fig. 10: MAE differences of considered models against the Stitch-BJ distribution fitted to ERA5-L over Metropolitan France

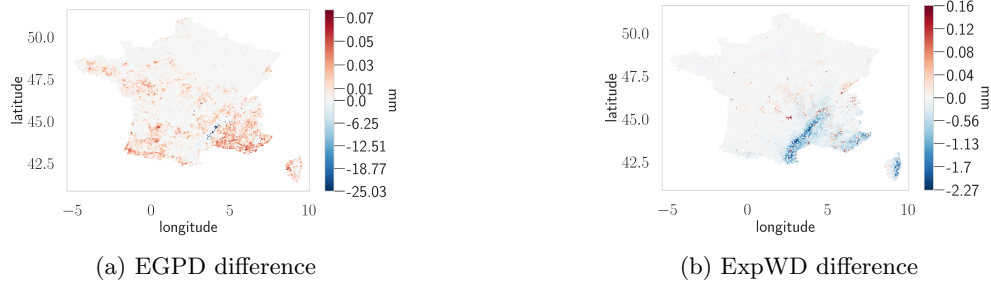
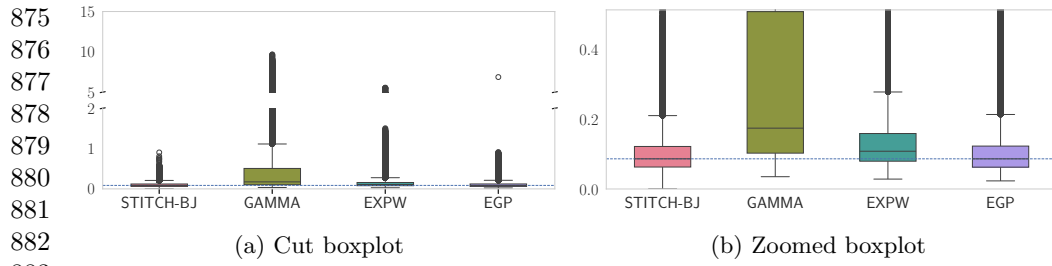


Fig. 11: MAE differences of considered models against the Stitch-BJ distribution fitted to CERRA-L over Metropolitan France

In the MAE in Figures 12 and 13, the impact of the Stitch-BJ method on extreme outliers are clear. The ExpW produces much less extreme outliers than the EGP on the CERRA-L data, however, the median error and the spread are much worse compared to both the EGP and the Stitch-BJ. The median error of the EGP and Stitch-BJ are very similar which is expected since the proposed inference procedure keeps as much EGP model in the final Stitch-BJ one as possible.



888
889
890
891
892
893
894
895
896
897
898
899
900
901
902
903
904
905
906
907
908
909
910
911
912
913
914
915
916
917
918
919
920

Fig. 12: Boxplots of MAE for considered models fit on ERA5-L

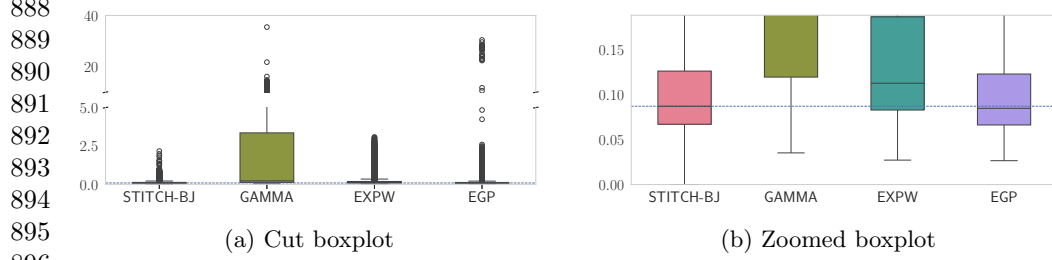


Fig. 13: Boxplots of MAE for considered models fit on CERRA-L

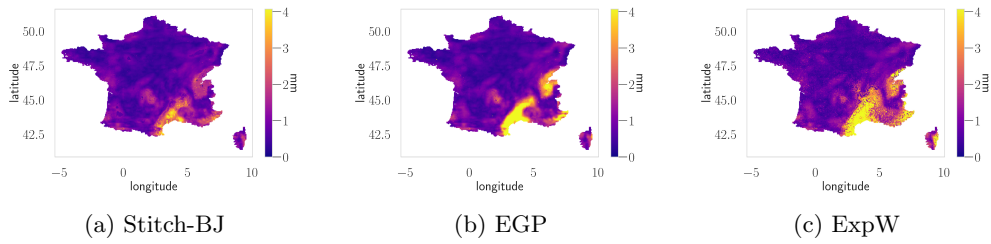


Fig. 14: MAE95sup of considered models fitted to ERA5-L over Metropolitan France.

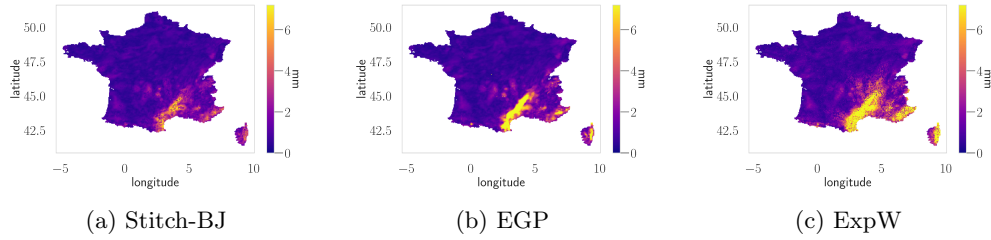


Fig. 15: MAE95sup of considered models fitted to CERRA-L over Metropolitan France

In Figures 14 and 15, we display the errors on the upper tail (See Appendix A). The improvements of the Stitch-BJ are further confirmed with a noticeable improvement over the Cévennes compared to all the other distributions, where the colour is not saturated compared to the EGPD and ExpWD for both ERA5-L and CERRA-L data.

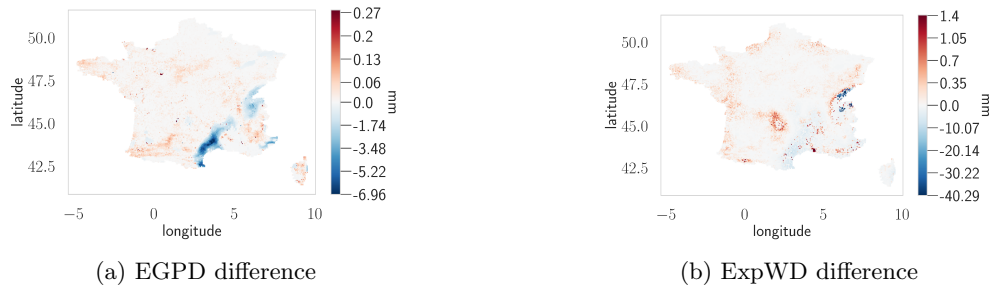


Fig. 16: MAE95sup differences of considered models against the Stitch-BJ distribution fitted to ERA5-L over Metropolitan France

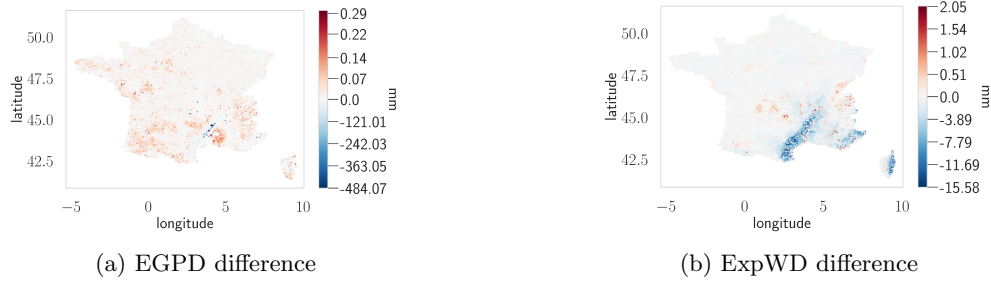


Fig. 17: MAE95sup differences of considered models against the Stitch-BJ distribution fitted to CERRA-L over Metropolitan France

921
922
923
924
925
926
927
928
929
930
931
932
933
934
935
936
937
938
939
940
941
942
943
944
945
946
947
948
949
950
951
952
953
954
955
956
957
958
959
960
961
962
963
964
965
966

967 Looking at Figures 16 and 17, the conclusion are very similar to Figures 10 and 11
 968 with the error range difference being even greater. The improvements by the Stitch-
 969 BJ can also be explained by the use of the empirical distribution on locations where
 970 the EGP produces completely inaccurate values.

971

972

973

974

975

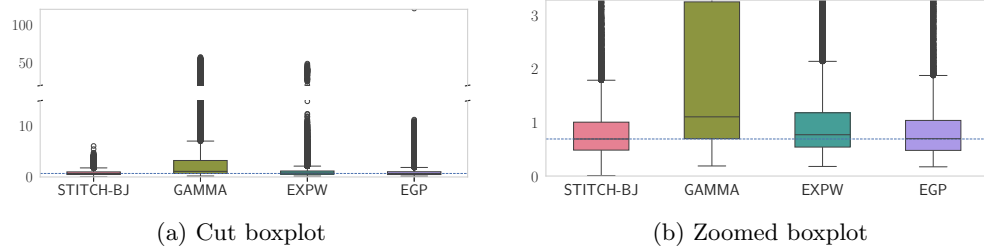
976

977

978

979

980



981 **Fig. 18:** Boxplots of MAE95sup for considered models fit on ERA5-L

982

983

984

985

986

987

988

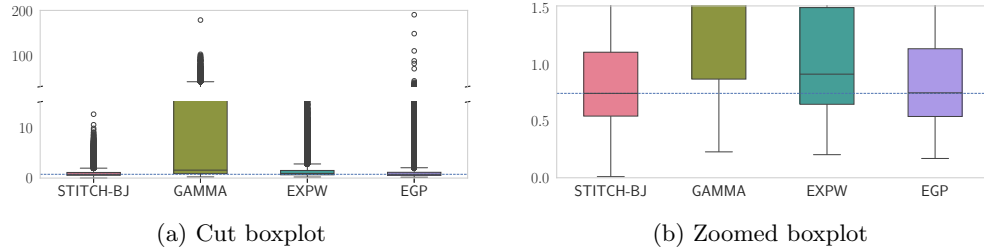
989

990

991

992

993



994 **Fig. 19:** Boxplot of MAE95sup for considered models fit on CERRA-L.

995

996

997

998

999

1000

1001

1002

1003

1004

1005

1006

4.2.2 Detailed analysis on selected locations

1007

1008

1009

1010

1011

1012

For a more precise study, we selected two locations in the Provence-Alpes-Côte d'Azur region to illustrate various study cases. The selected locations are near Cros (Longitude 3.80, Latitude 44.00) and Bézaudun-les-Alpes (Longitude 7.08, Latitude 43.82).

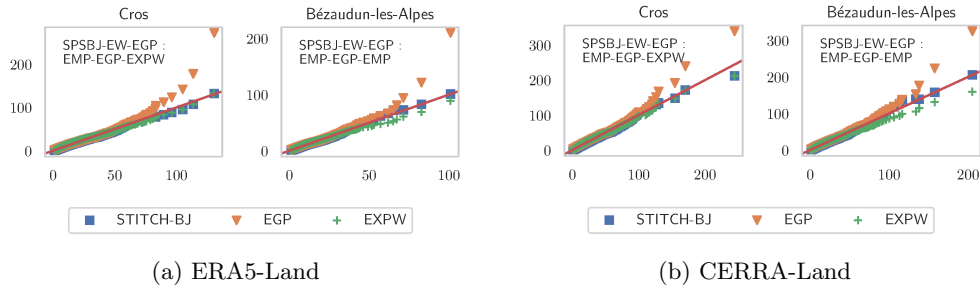


Fig. 20: QQ-plots of the Stitch-BJ (blue squares), EGP (red triangles) and ExpW (green crosses) fitted on ERA5-L and CERRA-L in the two selected locations

In Figure 20, the QQ-plots for the Stitch-BJ, ExpW and EGP models are shown, fitted for both ERA5-L and CERRA-L, for two different locations. For both ERA5-L and CERRA-L, the first location (Cros) shows a case where the upper tail is replaced by the ExpW, while the EGP is only used for the mid/high precipitation values. The other location, Bézaudun-les-Alpes, is a location where both parametric distributions were unable to correctly model the upper tail which result in the use of the empirical distribution for the extremes. While the ExpW exhibits visually a good fit for the upper tail on this location for both ERA5-L and CERRA-L, the deviation is enough to produce a rejection for the modified BJ test. For both locations and both datasets, neither parametric distribution was able to correctly model the lower tail, therefore it has been modelled using the empirical distribution.

4.3 Bias correction results

After fitting the Stitch-BJ and the other considered distributions on both ERA5-L and CERRA-L, we can now compare the performance of bias correction of the ERA5-L reanalysis against the CERRA-L reanalysis for the same period.

4.3.1 Spatialized metrics

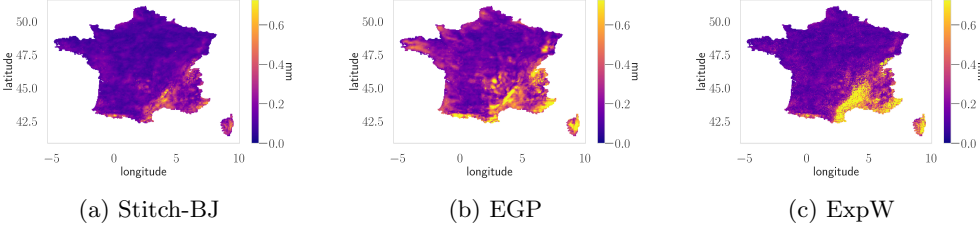
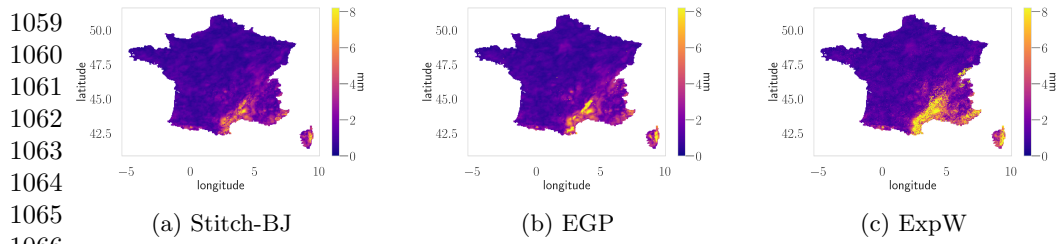


Fig. 21: MAE of considered models for the bias correction of ERA5-L using CERRA-L over Metropolitan France.



1067 **Fig. 22:** MAE95sup of considered models for the bias correction of ERA5-L using
1068 CERRA-L over Metropolitan France.

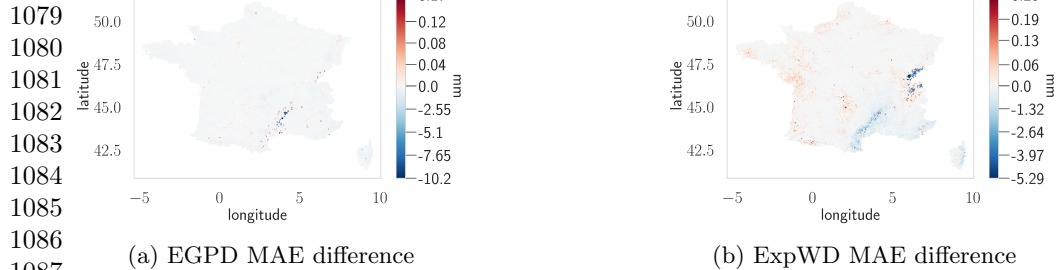
1069

1070

1071 Figures 21 and 22 show metrics (MAE and MAE95sup) for the bias correction error
1072 of ERA5-Land using CERRA-L. For both metrics, the Stitch-BJ produces the least
1073 extremes, both in number (spatially) and in intensity. The highest MAE is divided by
1074 3 when comparing the EGP and the Stitch-BJ model while the highest MAE95sup
1075 is improved from over 274mm (resp. 62mm) for the EGP (resp. ExpWD) to 12mm
1076 with the Stitch-BJ model.

1077

1078



1088 **Fig. 23:** MAE differences of considered models against the Stitch-BJ distribution for
1089 the bias correction of ERA5-L using CERRA-L over Metropolitan France

1090

1091

1092

1093

1094

1095

1096

1097

1098

1099

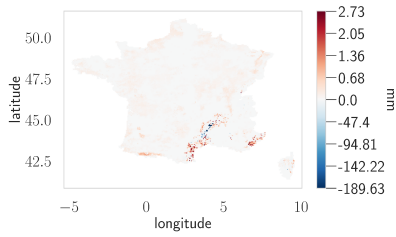
1100

1101

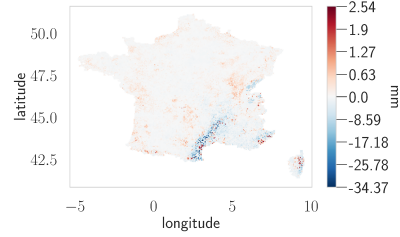
1102

1103

1104



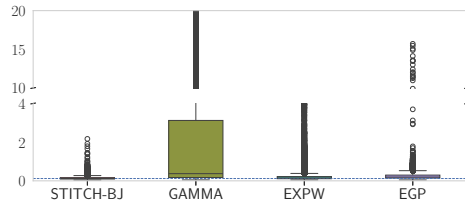
(a) EGPD MAE95sup difference



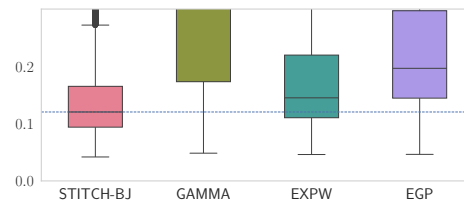
(b) ExpWD MAE95sup difference

Fig. 24: MAE95sup differences of considered models against the Stitch-BJ distribution for the bias correction of ERA5-L using CERRA-L over Metropolitan France

Figures 23 and 24 allow us to appreciate the impact of the correction spatially. Most of the Stitch-BJ improvements are located on the Cévennes and Alps region compared to respectively the EGPD and ExpWD.

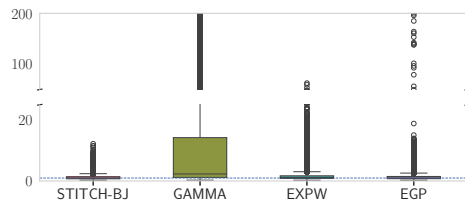


(a) Cut boxplot

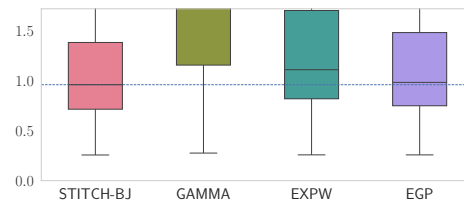


(b) Zoomed boxplot

Fig. 25: Boxplots of MAE for the bias corrected ERA5-L over CERRA-L for the considered models.



(a) Cut boxplot



(b) Zoomed boxplot

Fig. 26: Boxplots of MAE for the bias corrected ERA5-L over CERRA-L for the considered models

1151 Boxplots in Figures 25 and 26 confirm the previous observations, with both extremes
1152 and median MAE being greatly reduced compared to all the other tested distribu-
1153 tions. Median MAE95sup is not noticeably improved compared to the EGP, however
1154 extreme outliers are mostly corrected. Interestingly, while the ExpW model performed
1155 worse than the EGP one in terms of median error in the fit context, it actually
1156 outperforms the latter in the bias correction context for the MAE.

1157 After bias correction the maximum MAE (resp. MAE95sup) of the Stitch-BJ is
1158 more than 3 times (resp. 5 times) lower than the next model highest MAE (resp.
1159 MAE95sup).

1160

1161 5 Conclusion and discussion

1162

1163 In this study, we introduced a novel semi-parametric stitch distribution based on the
1164 BJ statistical test for daily precipitation modelling, which is able to automatically
1165 deduce cutting indexes and stitch our quantile functions and cdf. We then compared
1166 its fit and bias correction performance to the EGP, ExpW and Gamma distribution
1167 over the ERA5-L and CERRA-L reanalysis on France. We first conducted a short
1168 comparison of the ERA5-L and CERRA-L reanalysis in order to justify the need
1169 for bias correction. Our novel semi-parametric stitch distribution allows for a better
1170 representation of the extremes, either by using another parametric distribution, or by
1171 using the best known data available i.e. the empirical distribution.

1172 The Stitch-BJ distribution is constructed in 4 steps : (i) cutting indexes and rejection
1173 types are inferred for the EGP, (ii) same for the ExpWD and replace portions of the
1174 distribution accordingly, (iii) if neither parametric distributions are satisfactory, use
1175 the empirical distribution and (iv) classical properties (for instance monotonicity) of
1176 the cdf and quantile function are restored if they've been broken by the previous steps.
1177 Fit results shows that the model is able to find the right combination of distributions,
1178 resulting in large improvements over the EGP or ExpW model on the extremes, against
1179 a trade-off over lower and medium precipitations value. In a bias correction context, the
1180 Stitch-BJ method reduced the median MAE by respectively 20% and 40% compared
1181 to the ExpWD and EGP, and the maximum MAE by respectively 67% and 86%. The
1182 median MAE95sup was reduced by respectively 14% and 3.5%, while the maximum
1183 MAE95sup was reduced by respectively 80% and 95%.

1184 We conclude that the proposed Stitch-BJ distribution is able to improve the extremes
1185 against all the parametric distributions tested in this paper, making it a strong
1186 contender for rainfall modelling.

1187 However these results should be considered with care as the use of the empirical distri-
1188 bution on the tails or for the whole distribution on some locations may be responsible
1189 for the largest improvements seen. However, as we have seen in Figure 7 and Table 1,
1190 the empirical distribution is used in most around 9% of locations in the upper tail, and
1191 the replacement is mostly for the last 2 or 3% of the distribution (see Appendix D).

1192 This work allowed us to develop a flexible semi-parametric model for daily precipita-
1193 tion modelling, but many improvements and applications are yet to be done, from
1194 applications in a climate change context to modelling other climate variables using
1195 different distributions. Indeed, we used the empirical distribution when none of the
1196

proposed distributions were able to model the data with enough precision because it is the best performing model in a bias correction context when considering the same time-period. However, the performance in a climate change context may vary. This open interesting perspectives to perform a proper comparison of bias correction performance between parametric and empirical quantile mapping in a climate change context, using long enough time series to be able to split them. One may also want to completely remove the implication of the empirical distribution by involving more parametric distributions.

Data availability: All data, material, and programming codes used in this study are available upon request. ERA5-Land and CERRA-Land datasets analyzed in the current study are available on the [Copernicus Climate Change Service \(C3S\) Climate Data Store](#).

Acknowledgments: This work has been partially supported by the French government through the 3IA Côte d’Azur Investments in the Future project managed by the National Research Agency (ANR-19-P3IA-0002).

References

- Anderson, T.W., Darling, D.A.: A Test of Goodness of Fit. *Journal of the American Statistical Association* **49**(268), 765–769 (1954) <https://doi.org/10.1080/01621459.1954.10501232> . Publisher: Taylor & Francis .eprint: <https://www.tandfonline.com/doi/pdf/10.1080/01621459.1954.10501232>. Accessed 2024-04-23
- Acero, F.J., García, J.A., Gallego, M.C.: Peaks-over-Threshold Study of Trends in Extreme Rainfall over the Iberian Peninsula. *Journal of Climate* **24**(4), 1089–1105 (2011) <https://doi.org/10.1175/2010JCLI3627.1> . Publisher: American Meteorological Society Section: *Journal of Climate*. Accessed 2023-05-16
- Anderson, T.W.: On the Distribution of the Two-Sample Cramer-von Mises Criterion. *The Annals of Mathematical Statistics* **33**(3), 1148–1159 (1962) <https://doi.org/10.1214/aoms/1177704477> . Publisher: Institute of Mathematical Statistics. Accessed 2024-04-23
- Alferi, L., Thielen, J.: A European precipitation index for extreme rain-storm and flash flood early warning. *Meteorological Applications* **22**(1), 3–13 (2015) <https://doi.org/10.1002/met.1328> . .eprint: <https://onlinelibrary.wiley.com/doi/pdf/10.1002/met.1328>. Accessed 2023-05-17
- Balkema, A.A., Haan, L.d.: Residual Life Time at Great Age. *The Annals of Probability* **2**(5), 792–804 (1974) <https://doi.org/10.1214/aop/1176996548> . Publisher: Institute of Mathematical Statistics. Accessed 2024-04-24
- Berk, R.H., Jones, D.H.: Goodness-of-fit test statistics that dominate the Kolmogorov

1243 statistics. *Zeitschrift für Wahrscheinlichkeitstheorie und Verwandte Gebiete* **47**(1),
 1244 47–59 (1979) <https://doi.org/10.1007/BF00533250> . Accessed 2024-01-23
 1245
 1246 Blain, G.C., Meschiatti, M.C.: Inadequacy of the Gamma distribution to calculate
 1247 the Standardized Precipitation Index. *Revista Brasileira de Engenharia Agrícola*
 1248 *e Ambiental* **19**, 1129–1135 (2015) <https://doi.org/10.1590/1807-1929/agriambi.v19n12p1129-1135> . Publisher: Departamento de Engenharia Agrícola - UFCG.
 1249 Accessed 2023-05-16
 1250
 1251 C3S: ERA5 hourly data on single levels from 1940 to present (2018). <https://doi.org/10.24381/CDS.ADBB2D47> . <https://cds.climate.copernicus.eu/doi/10.24381/cds.adbb2d47> Accessed 2024-04-05
 1252
 1253 Castro-Camilo, D., Huser, R., Rue, H.: A Spliced Gamma-Generalized Pareto Model
 1254 for Short-Term Extreme Wind Speed Probabilistic Forecasting. *Journal of Agricultural, Biological and Environmental Statistics* **24**(3), 517–534 (2019) <https://doi.org/10.1007/s13253-019-00369-z> . Accessed 2024-07-08
 1255
 1256 Chen, D., Dai, A., Hall, A.: The Convective-To-Total Precipitation Ratio and the
 1257 “Drizzling” Bias in Climate Models. *Journal of Geophysical Research: Atmospheres* **126**(16), 2020–034198 (2021) <https://doi.org/10.1029/2020JD034198> .
 1258 eprint: <https://onlinelibrary.wiley.com/doi/pdf/10.1029/2020JD034198>. Accessed
 1259 2024-07-08
 1260
 1261 Carrió, D.S., Jansà, A., Homar, V., Romero, R., Rigo, T., Ramis, C., Hermoso,
 1262 A., Maimó, A.: Exploring the benefits of a Hi-EnKF system to forecast an
 1263 extreme weather event. The 9th October 2018 catastrophic flash flood in Mallorca.
 1264 *Atmospheric Research* **265**, 105917 (2022) <https://doi.org/10.1016/j.atmosres.2021.105917> . Accessed 2023-05-16
 1265
 1266 Costache, R., Tien Bui, D.: Identification of areas prone to flash-flood phenomena
 1267 using multiple-criteria decision-making, bivariate statistics, machine learning and
 1268 their ensembles. *Science of The Total Environment* **712**, 136492 (2020) <https://doi.org/10.1016/j.scitotenv.2019.136492> . Accessed 2023-05-16
 1269
 1270 Cucchi, M., Weedon, G., Amici, A., Bellouin, N., Lange, S., Müller Schmied, H.,
 1271 Hersbach, H., Buontempo, C.: WFDE5: bias adjusted ERA5 reanalysis data for
 1272 impact studies (2020) <https://doi.org/10.5194/essd-12-2097-2020>
 1273
 1274 De Haan, L., Ferreira, A.: *Extreme Value Theory*. Springer Series in Operations
 1275 Research and Financial Engineering. Springer, New York, NY (2006). <https://doi.org/10.1007/0-387-34471-3> . <http://link.springer.com/10.1007/0-387-34471-3>
 1276 Accessed 2024-07-09
 1277
 1278 Déqué, M.: Frequency of precipitation and temperature extremes over France in
 1279 an anthropogenic scenario: Model results and statistical correction according to
 1280 observed values. *Global and Planetary Change* **57**(1), 16–26 (2007) <https://doi.org/>
 1281
 1282
 1283
 1284
 1285
 1286
 1287
 1288

10.1016/j.gloplacha.2006.11.030 . Accessed 2023-02-06	1289
Gamet, P., Jالبert, J.: A flexible Extended Generalized Pareto distribution for tail estimation. <i>Environmetrics</i> 33 (6), 2744 (2022) https://doi.org/10.1002/env.2744 .	1290
_eprint: https://onlinelibrary.wiley.com/doi/pdf/10.1002/env.2744 . Accessed 2023-	1291
10-17	1292
Henckes, P., Knaut, A., Obermüller, F., Frank, C.: The benefit of long-term high resolution wind data for electricity system analysis. <i>Energy</i> 143 , 934–942 (2018)	1293
https://doi.org/10.1016/j.energy.2017.10.049 . Accessed 2023-05-03	1294
Husak, G.J., Michaelsen, J.C., Funk, C.C.: Use of the Gamma distribution to represent monthly rainfall in Africa for drought monitoring applications. <i>International Journal of Climatology</i> 27 (7), 935–944 (2007) https://doi.org/10.1002/joc.1441 . Accessed	1295
2024-06-12	1296
Katz, R.W.: Techniques for estimating uncertainty in climate change scenarios and impact studies. <i>Climate Research</i> 20 (2), 167–185 (2002) https://doi.org/10.3354/cr020167 . Accessed 2024-06-12	1297
Khan, S.A.: Exponentiated Weibull regression for time-to-event data. <i>Lifetime Data Analysis</i> 24 (2), 328–354 (2018) https://doi.org/10.1007/s10985-017-9394-3 .	1298
Accessed 2024-01-29	1299
Kim, Y., Kim, H., Lee, G., Min, K.-H.: A Modified Hybrid Gamma and Generalized Pareto Distribution for Precipitation Data. <i>Asia-Pacific Journal of Atmospheric Sciences</i> 55 (4), 609–616 (2019) https://doi.org/10.1007/s13143-019-00114-z . Accessed	1300
2024-07-08	1301
Laio, F.: Cramer–von Mises and Anderson-Darling goodness of fit tests for extreme value distributions with unknown parameters. <i>Water Resources Research</i> 40 (9) (2004) https://doi.org/10.1029/2004WR003204 . _eprint: https://onlinelibrary.wiley.com/doi/pdf/10.1029/2004WR003204 . Accessed	1302
2024-06-12	1303
Lafon, T., Dadson, S., Buys, G., Prudhomme, C.: Bias correction of daily precipitation simulated by a regional climate model: a comparison of methods. <i>International Journal of Climatology</i> 33 (6), 1367–1381 (2013) https://doi.org/10.1002/joc.3518 . _eprint: https://onlinelibrary.wiley.com/doi/pdf/10.1002/joc.3518 . Accessed 2023-	1304
05-03	1305
Li, B., Huang, Y., Du, L., Wang, D.: Bias Correction for Precipitation Simulated by RegCM4 over the Upper Reaches of the Yangtze River Based on the Mixed Distribution Quantile Mapping Method. <i>Atmosphere</i> 12 (12), 1566 (2021) https://doi.org/10.3390/atmos12121566 . Number: 12 Publisher: Multidisciplinary Digital Publishing Institute. Accessed 2023-03-28	1306
	1307
	1308
	1309
	1310
	1311
	1312
	1313
	1314
	1315
	1316
	1317
	1318
	1319
	1320
	1321
	1322
	1323
	1324
	1325
	1326
	1327
	1328
	1329
	1330
	1331
	1332
	1333
	1334

1335 Li, C., Singh, V.P., Mishra, A.K.: Simulation of the entire range of daily
1336 precipitation using a hybrid probability distribution. *Water Resources*
1337 *Research* **48**(3) (2012) <https://doi.org/10.1029/2011WR011446> . eprint:
1338 <https://onlinelibrary.wiley.com/doi/pdf/10.1029/2011WR011446>. Accessed
1339 2023-09-20
1340
1341 Massey Jr., F.J.: The Kolmogorov-Smirnov Test for Goodness of Fit. *Journal of the American Statistical Association* **46**(253), 68–78 (1951) <https://doi.org/10.1080/01621459.1951.10500769> . Publisher: Taylor & Francis eprint:
1342 <https://www.tandfonline.com/doi/pdf/10.1080/01621459.1951.10500769>. Accessed
1343 2024-04-23
1344
1345
1346
1347 Monteiro, D., Morin, S.: Multi-decadal analysis of past winter temperature, precipi-
1348 tation and snow cover data in the European Alps from reanalyses, climate models
1349 and observational datasets. *The Cryosphere* **17**(8), 3617–3660 (2023) <https://doi.org/10.5194/tc-17-3617-2023> . Publisher: Copernicus GmbH. Accessed 2024-04-05
1350
1351
1352 Moscovich, A., Nadler, B.: Fast calculation of boundary crossing probabilities for
1353 Poisson processes. *Statistics & Probability Letters* **123**, 177–182 (2017) <https://doi.org/10.1016/j.spl.2016.11.027> . Accessed 2024-01-23
1354
1355
1356 Moscovich, A., Nadler, B., Spiegelman, C.: On the exact Berk-Jones statistics and
1357 their p-value calculation. *Electronic Journal of Statistics* **10**(2) (2016) <https://doi.org/10.1214/16-EJS1172> . arXiv:1311.3190 [math, stat]. Accessed 2023-11-26
1358
1359
1360 Moscovich, A.: Fast calculation of p-values for one-sided Kolmogorov-Smirnov type
1361 statistics. *Computational Statistics & Data Analysis* **185**, 107769 (2023) <https://doi.org/10.1016/j.csda.2023.107769> . Accessed 2024-01-25
1362
1363
1364 Mudholkar, G.S., Srivastava, D.K.: Exponentiated Weibull family for analyzing bath-
1365 tub failure-rate data. *IEEE Transactions on Reliability* **42**(2), 299–302 (1993) <https://doi.org/10.1109/24.229504> . Conference Name: IEEE Transactions on Reliability.
1366 Accessed 2023-11-16
1367
1368
1369 Muñoz-Sabater, J., Dutra, E., Agustí-Panareda, A., Albergel, C., Arduini, G., Bal-
1370 samo, G., Bousssetta, S., Choulga, M., Harrigan, S., Hersbach, H., Martens, B.,
1371 Miralles, D.G., Piles, M., Rodríguez-Fernández, N.J., Zsoter, E., Buontempo, C.,
1372 Thépaut, J.-N.: ERA5-Land: a state-of-the-art global reanalysis dataset for land
1373 applications. *Earth System Science Data* **13**(9), 4349–4383 (2021) <https://doi.org/10.5194/essd-13-4349-2021> . Publisher: Copernicus GmbH. Accessed 2023-05-02
1374
1375
1376 Mudholkar, G.S., Srivastava, D.K., Kollia, G.D.: A Generalization of the Weibull Dis-
1377 tribution with Application to the Analysis of Survival Data. *Journal of the American*
1378 *Statistical Association* **91**(436), 1575–1583 (1996) <https://doi.org/10.2307/2291583>
1379 . Publisher: [American Statistical Association, Taylor & Francis, Ltd.]. Accessed
1380 2024-01-29

Malaekheh, S., Safaie, A., Shiva, L., Tabari, H.: Spatio-temporal variation of hydro-climatic variables and extreme indices over Iran based on reanalysis data. *Stochastic Environmental Research and Risk Assessment* **36**(11), 3725–3752 (2022) <https://doi.org/10.1007/s00477-022-02223-0> . Accessed 2024-04-05

McNeil, A., Saladin, T., Zentrum, E.: The Peaks over Thresholds Method for Estimating High Quantiles of Loss Distributions. *Proceedings of 28th International ASTIN Colloquium* (1997)

Martinez-Villalobos, C., Neelin, J.D.: Why Do Precipitation Intensities Tend to Follow Gamma Distributions? *Journal of the Atmospheric Sciences* **76**(11), 3611–3631 (2019) <https://doi.org/10.1175/JAS-D-18-0343.1> . Publisher: American Meteorological Society Section: *Journal of the Atmospheric Sciences*. Accessed 2023-03-28

Nadarajah, S., Choi, D.: Maximum daily rainfall in South Korea. *Journal of Earth System Science* **116**(4), 311–320 (2007) <https://doi.org/10.1007/s12040-007-0028-0> . Accessed 2024-01-29

Naveau, P., Huser, R., Ribereau, P., Hannart, A.: Modeling jointly low, moderate, and heavy rainfall intensities without a threshold selection. *Water Resources Research* **52**(4), 2753–2769 (2016) <https://doi.org/10.1002/2015WR018552> . eprint: <https://onlinelibrary.wiley.com/doi/pdf/10.1002/2015WR018552>. Accessed 2023-09-20

Pal, M., Ali, M.M., Woo, J.: Exponentiated Weibull distribution. *Statistica* **66**(2), 139–147 (2006) <https://doi.org/10.6092/issn.1973-2201/493> . Number: 2. Accessed 2024-01-29

Prein, A.F., Gobiet, A., Truhetz, H., Keuler, K., Goergen, K., Teichmann, C., Fox Maule, C., Meijgaard, E., Déqué, M., Nikulin, G., Vautard, R., Colette, A., Kjellström, E., Jacob, D.: Precipitation in the EURO-CORDEX 0.11° and 0.44° simulations: high resolution, high benefits? *Climate Dynamics* **46**(1), 383–412 (2016) <https://doi.org/10.1007/s00382-015-2589-y> . Accessed 2023-05-03

Pickands, J.I.: Statistical Inference Using Extreme Order Statistics. *The Annals of Statistics* **3**(1), 119–131 (1975) <https://doi.org/10.1214/aos/1176343003> . Publisher: Institute of Mathematical Statistics. Accessed 2024-04-24

Papastathopoulos, I., Tawn, J.A.: Extended generalised Pareto models for tail estimation. *Journal of Statistical Planning and Inference* **143**(1), 131–143 (2013) <https://doi.org/10.1016/j.jspi.2012.07.001> . Accessed 2023-09-20

Ristić, M.M., Balakrishnan, N.: The Gamma-Exponentiated Exponential distribution. *Journal of Statistical Computation and Simulation* **82**(8), 1191–1206 (2012) <https://doi.org/10.1080/00949655.2011.574633> . Publisher: Taylor & Francis eprint: <https://doi.org/10.1080/00949655.2011.574633>. Accessed 2024-01-29

1427 Rootzén, H., Tajvidi, N.: Extreme value statistics and wind storm losses: A
1428 case study. *Scandinavian Actuarial Journal* **1997**(1), 70–94 (1997) <https://doi.org/10.1080/03461238.1997.10413979> . Publisher: Taylor & Francis .eprint:
1429 <https://doi.org/10.1080/03461238.1997.10413979> . Accessed 2023-05-03
1430
1431
1432 Sangati, M., Borga, M.: Influence of rainfall spatial resolution on flash flood modelling.
1433 *Natural Hazards and Earth System Sciences* **9**(2), 575–584 (2009) <https://doi.org/10.5194/nhess-9-575-2009> . Publisher: Copernicus GmbH. Accessed 2023-05-17
1434
1435
1436 Soares, P.M.M., Cardoso, R.M.: A simple method to assess the added
1437 value using high-resolution climate distributions: application to the
1438 EURO-CORDEX daily precipitation. *International Journal of Climatol-*
1439 *ogy* **38**(3), 1484–1498 (2018) <https://doi.org/10.1002/joc.5261> . .eprint:
1440 <https://onlinelibrary.wiley.com/doi/pdf/10.1002/joc.5261>. Accessed 2023-05-03
1441
1442 Sharma, V.K., Singh, S.V., Shekhawat, K.: Exponentiated Teissier distribution with
1443 increasing, decreasing and bathtub hazard functions. *Journal of Applied Statistics*
1444 **49**(2), 371–393 (2022) <https://doi.org/10.1080/02664763.2020.1813694> . Publisher:
1445 Taylor & Francis .eprint: <https://doi.org/10.1080/02664763.2020.1813694>. Accessed
1446 2024-01-29
1447
1448 Steinskog, D.J., Tjøstheim, D.B., Kvamstø, N.G.: A Cautionary Note on the Use of the
1449 Kolmogorov–Smirnov Test for Normality. *Monthly Weather Review* **135**(3), 1151–
1450 1157 (2007) <https://doi.org/10.1175/MWR3326.1> . Publisher: American Meteorological Society Section: Monthly Weather Review. Accessed 2024-06-12
1451
1452 Tencaliec, P., Favre, A.-C., Naveau, P., Prieur, C., Nicolet, G.: Flexible semiparametric
1453 Generalized Pareto modeling of the entire range of rainfall amount. *Environmetrics*
1454 **31**(2), 2582–1 (2019) <https://doi.org/10.1002/env.2582> . Accessed 2023-10-12
1455
1456 The MathWorks Inc.: MATLAB. The MathWorks Inc., Natick, Massachusetts, United
1457 States (2022). <https://www.mathworks.com>
1458
1459 Verrelle, A., Glinton, M., Bazile, E., Moigne, P.L.: CERRA-Land : A new land
1460 surface reanalysis at 5.5 km resolution over Europe. Technical Report EMS2021-
1461 492, Copernicus Meetings (June 2021). <https://doi.org/10.5194/ems2021-492> .
1462 Conference Name: EMS2021. [https://meetingorganizer.copernicus.org/EMS2021/](https://meetingorganizer.copernicus.org/EMS2021/EMS2021-492.html)
1463 [EMS2021-492.html](https://meetingorganizer.copernicus.org/EMS2021/EMS2021-492.html) Accessed 2024-03-21
1464
1465 Vlček, O., Huth, R.: Is daily precipitation Gamma-distributed?: Adverse effects of an
1466 incorrect use of the Kolmogorov–Smirnov test. *Atmospheric Research* **93**(4), 759–
1467 766 (2009) <https://doi.org/10.1016/j.atmosres.2009.03.005> . Accessed 2023-03-28
1468
1469 Xu, H., Xu, C.-Y., Sælthun, N.R., Zhou, B., Xu, Y.: Evaluation of reanalysis and
1470 satellite-based precipitation datasets in driving hydrological models in a humid
1471 region of Southern China. *Stochastic Environmental Research and Risk Assessment*
1472 **29**(8), 2003–2020 (2015) <https://doi.org/10.1007/s00477-014-1007-z> . Accessed

Yang, F., Koukoulou, M., Emmanouil, S., Cerrai, D., Anagnostou, E.N.: Assessing the power grid vulnerability to extreme weather events based on long-term atmospheric reanalysis. *Stochastic Environmental Research and Risk Assessment* **37**(11), 4291–4306 (2023) <https://doi.org/10.1007/s00477-023-02508-y> . Accessed 2024-07-08

Yue, Z., Xiong, L., Zha, X., Liu, C., Chen, J., Liu, D.: Impact of thresholds on nonstationary frequency analyses of peak over threshold extreme rainfall series in Pearl River Basin, China. *Atmospheric Research* **276**, 106269 (2022) <https://doi.org/10.1016/j.atmosres.2022.106269> . Accessed 2023-05-16

Şan, M., Nacar, S., Kankal, M., Bayram, A.: Daily precipitation performances of regression-based statistical downscaling models in a basin with mountain and semi-arid climates. *Stochastic Environmental Research and Risk Assessment* **37**(4), 1431–1455 (2023) <https://doi.org/10.1007/s00477-022-02345-5> . Accessed 2024-07-08

A Considered metrics

To quantify and spatially visualise fit and bias correction errors of our distributional models and data, we selected two metrics: one taking into account the whole distribution (MAE) and the other one focused on the upper tail (MAE95sup, i.e., the MAE over the 5th last quantile).

Let $q = \{q_1 = 0, q_2 = \frac{1}{n}, \dots, q_n = 1 - \frac{1}{n}\}$, with $n = 1000$. For faster computation times and standardization, we produce an equally spaced quantile representation of the target and prediction data using q . The quantile function used is from Python's `numpy` package, with the linear interpolation method.

The ordered data quantiles are noted y and \hat{y} for respectively x_{obs} and x_{mod} , the observed and modelled data.

The Mean Absolute Error is defined as:

$$MAE = \frac{1}{n} \sum_{i=1}^n |y_{(i)} - \hat{y}_{(i)}|.$$

The Mean Absolute Error over quantile α (MAE α sup) is derived from the MAE to focus on the upper tail. More precisely, it is the MAE over the quantile α . It is defined as:

$$MAE\alpha\text{sup} = \frac{1}{n - \lceil \alpha \times n \rceil} \sum_{i=\lceil \alpha \times n \rceil}^n |y_{(i)} - \hat{y}_{(i)}|,$$

with $\lceil x \rceil$ being the ceiling function.

1519 **B Considered parametric distributions**

1520

1521 We introduce some parametric distributions: the Extended Generalized Pareto (EGP)
1522 distribution, the Exponentiated Weibull (ExpW) distribution and the Gamma distri-
1523 bution. The first two distributions are used to construct our semi-parametric model
1524 and the Gamma distribution is used for comparisons.

1525 Note that for precipitation modelling, we used a 1mm threshold to separate between
1526 wet and dry days. The support of the following distributions being $]0, +\infty[$, a shift of
1527 1mm has been applied before fitting, since the wet days threshold chosen is also 1mm.

1528

1529 **The Gamma distribution**

1530 The Gamma distribution is a well-known light-tailed and often used distribution for
1531 daily and monthly precipitation modelling (Martinez-Villalobos and Neelin, 2019;
1532 Husak et al., 2007). Its cumulative distribution function can be written as:

1533

1534

$$F(x) = \frac{1}{\Gamma(k)} \gamma(\alpha, \beta x),$$

1535

1536 for $x > 0$ and $\alpha > 0$ and $\beta > 0$ respectively the shape and rate parameters.

1537

1538 **The Extended Generalized Pareto distribution**

1539

1540 An extension of the Generalized Pareto distribution have been introduced in Naveau
1541 et al. (2016); Papastathopoulos and Tawn (2013). This extension removes the difficult
1542 choice of the threshold for the classical generalized Pareto distribution (GPD).

1543 The distribution has the following form:

1544

1545

1546

$$F_{EGP}(x; G) = \begin{cases} G \left(1 - (1 + \xi x / \sigma)^{-\frac{1}{\xi}} \right), & \xi > 0, \\ G \left(1 - e^{-\frac{x}{\sigma}} \right), & \xi = 0, \end{cases} \quad (\text{B.1})$$

1547

1548

1549 with σ and ξ being the usual parameters of the GPD distribution, and G a continuous
1550 cumulative distribution function on $[0, 1]$ to that fulfils the necessary conditions from
1551 Naveau et al. (2016).

1552 In the aforementioned article, multiple distributions for G have been presented that
1553 satisfy the required conditions. In this paper, we will focus on the first model denoted
1554 by EGP, which uses the power law distribution: $G(x) = x^\kappa$, for κ and $x > 0$, i.e.,

1555

1556

1557

1558

$$F_{EGP}(x) = \begin{cases} \left(1 - (1 + \xi x / \sigma)^{-\frac{1}{\xi}} \right)^\kappa, & \xi > 0, \\ \left(1 - e^{-\frac{x}{\sigma}} \right)^\kappa, & \xi = 0. \end{cases}$$

1559 Left censoring can also be applied when fitting the distribution (more information on
1560 the censoring can be found in the original article Naveau et al. (2016)). We fixed at
1561 3mm the left censoring in our application in Section 3.

1562

1563

1564

Exponentiated Weibull distribution

The Exponentiated Weibull (ExpW) distribution has been introduced by [Mudholkar and Srivastava \(1993\)](#) and generalizes the Weibull distribution by adding a second parameter shape. Its cumulative distribution function can be written as:

$$F(x; k, \lambda, \alpha) = [1 - \exp(-(x/\lambda)^k)]^\alpha,$$

for $x > 0$ and $k, \alpha, \lambda > 0$ being respectively the first and second shape parameter and the scale parameter of the distribution. Taking $\alpha = 1$ gives the usual Weibull distribution and $k = 1$ gives the Exponentiated distribution.

The Exponentiated Weibull distribution has been used historically for failure rates ([Khan, 2018](#); [Pal et al., 2006](#)) and survival data modelisation ([Mudholkar et al., 1996](#)), but has also been used in some cases to model precipitation data ([Nadarajah and Choi, 2007](#); [Sharma et al., 2022](#); [Ristić and Balakrishnan, 2012](#)).

C Monotonicity correction and analytical description of the proposed semi-parametric distributional model

Replacing a portion of the quantile function with the empirical quantile function or the lighter-tailed $F_{lighter}$ quantile function should be done carefully. Since the quantile function is an increasing function, corrections may be needed to guarantee the monotonicity. To solve this issue, we introduce in the next section a modification for all locations.

C.1 Monotonicity correction and application

Let F_1 and F_2 two distribution functions non-decreasing and right-continuous with associated quantile functions F_1^{-1} and F_2^{-1} . We define \tilde{F}^{-1} as the following constructed pseudo-quantile function

$$\tilde{F}^{-1}(p) = \begin{cases} F_1^{-1}(p), & \forall p \leq p_{stitch}, \\ F_2^{-1}(p), & \text{otherwise,} \end{cases}$$

for $p_{stitch} \in [0, 1]$. Notice that the monotonicity condition of \tilde{F}^{-1} is not guaranteed. A breakage in the monotonicity of the pseudo-quantile function \tilde{F}^{-1} at probability p_{stitch} is characterized by the following condition:

$$\exists \epsilon > 0 \mid \tilde{F}^{-1}(p_{stitch}) > \tilde{F}^{-1}(p_{stitch} + \epsilon), \text{ i.e.,} \\ F_1^{-1}(p_{stitch}) > \lim_{\epsilon \rightarrow 0^+} F_2^{-1}(p_{stitch} + \epsilon).$$

We will consider two types of breaks: small breaks (with amplitude smaller than 5 mm) and large breaks with amplitude larger than 5 mm. This amplitude of 5mm was chosen arbitrarily in the present work and can be modified.

1611 In the first case, the correction is a shift on all values higher than the breaking point
 1612 quantile $F_1^{-1}(p_{\text{stitch}})$,

$$1613 \quad \tilde{F}^{-1}(p) = F_2^{-1}(p) + \underbrace{F_1^{-1}(p_{\text{stitch}}) - \lim_{\epsilon \rightarrow 0^+} F_2^{-1}(p_{\text{stitch}} + \epsilon)}_C, \forall p > p_{\text{stitch}}. \quad (\text{C.1})$$

1617 In the second case, the values produced by F_1^{-1} near p_{stitch} are considered as too high
 1618 and they might significantly change the quantile function if the correction in Equation
 1619 (C.1) is applied. In this second case, a type of ceiling function is applied to the values
 1620 produced by F_1 for all probabilities lower than the breakage point:

$$1622 \quad \tilde{F}^{-1}(p) = \min \left\{ F_1^{-1}(p), \underbrace{\lim_{\epsilon \rightarrow 0^+} F_2^{-1}(p_{\text{stitch}} + \epsilon)}_{C_{\text{ceil}}} \right\}, \quad \forall p \leq p_{\text{stitch}}. \quad (\text{C.2})$$

1625 Using these corrections on \tilde{F}^{-1} , the resulting quantile function is well-defined.

1628 **Application 4** Correction of monotonicity

- 1629 **Step (1)** Find the breaking point index i (either $i_{\ell,EGP}, i_{u,EGP}, i_{\ell,ExpW}$ or $i_{u,ExpW}$.
 1630 If there is more than one break in the pseudo-quantile function, the corrections
 1631 should be applied in ascending order (lower indexes first) and are cumulative.
 1632 **Step (2)** Determine the amplitude of the break η defined by $q_{(i-1)} - q_{(i)}$
 1633 **Step (3)** If $\eta \leq 5$, correct the monotonicity by shifting all values on the right of
 1634 the breaking point by the amplitude η as described in Equation (C.1).
 1635 **Step (4)** If $\eta > 5$, correct the monotonicity break by mapping those values to $x_{(i)}$
 1636 for all indices lower than i as in Equation (C.2).
-

1638
 1639
 1640
 1641
 1642
 1643
 1644
 1645
 1646
 1647
 1648
 1649
 1650
 1651
 1652
 1653
 1654
 1655
 1656

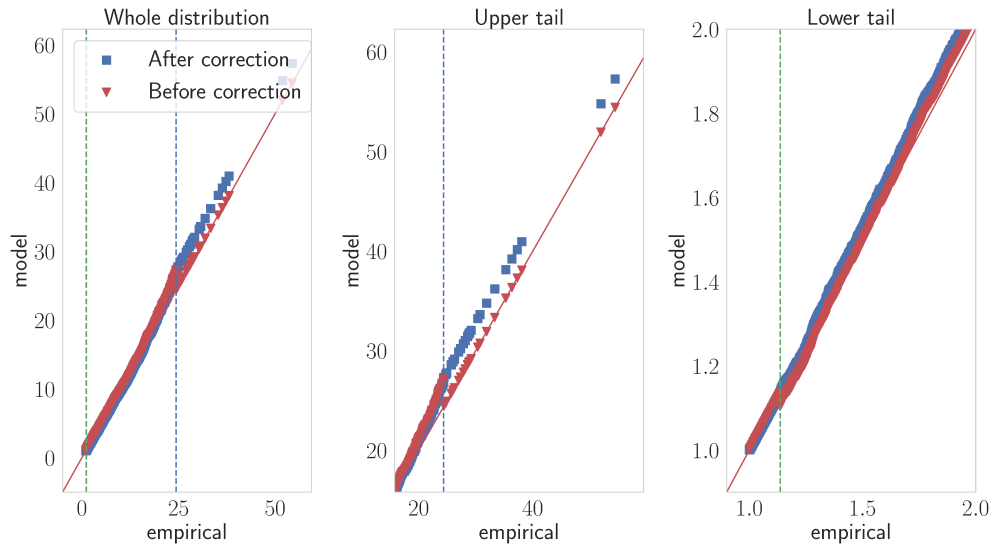


Fig. 27: QQ-plots of a location where the monotonicity has been broken on both the lower and upper cutting index

In Figure 27, both types of break in monotonicity have been corrected. In the lower quantiles (right panel), the break have been corrected by shifting all following values using Equation (C.1). In the higher quantiles (center panel), the break has been corrected using (C.1) as well thus shifting the values to obtain the monotonicity. If the break was greater than $\eta = 5$, the correction using (C.2) would have been used. From the newly corrected quantile function, it is now possible to properly define a proper cdf.

We can now give an analytical description for both the resulting stitched quantile function and associated cdf which will allow for both interpolation and extrapolation on unobserved values where the empirical distribution has not been stitched.

C.2 Analytical model

A semi-continuous description of the Stitch-BJ distribution can be derived using the cutting indexes and rejection types $i_{u,F}$, $i_{\ell,F}$ and typeRej_F for F_{heavy} and $F_{lighter}$ as defined in Definitions 1 and 2, and the booleans r_{all} , r_{left} and r_{right} as defined in Definition 3. In Definition 2, we have at most three different quantile functions used to describe infer the Stitch-BJ model. Let us define F_1^{-1} , F_2^{-1} and F_3^{-1} , three potentially identical quantile functions as follows:

1657
1658
1659
1660
1661
1662
1663
1664
1665
1666
1667
1668
1669
1670
1671
1672
1673
1674
1675
1676
1677
1678
1679
1680
1681
1682
1683
1684
1685
1686
1687
1688
1689
1690
1691
1692
1693
1694
1695
1696
1697
1698
1699
1700
1701
1702

1703

1704

1705

1706

1707

1708

1709

$$F_1^{-1} = \begin{cases} F_n^{-1}, & \text{if } \text{typeRej}_{F_{heavy}} \text{ and } \text{typeRej}_{F_{lighter}} == 2, 4 \text{ or } 5 \\ F_{lighter}^{-1}, & \text{if } r_{left} \text{ is True, or } r_{all} \text{ is True and } \text{typeRej}_{F_{lighter}} \neq 2 \text{ or } 4 \\ F_{heavy}^{-1}, & \text{otherwise} \end{cases} \quad (\text{C.3})$$

1710

1711

1712

1713

$$F_2^{-1} = \begin{cases} F_n^{-1}, & \text{if } r_{all} \text{ is False and } \text{typeRej}_{F_{heavy}} == 5 \\ F_{lighter}^{-1}, & \text{if } r_{all} \text{ is True} \\ F_{heavy}^{-1}, & \text{if } r_{all} \text{ is False and } \text{typeRej}_{F_{heavy}} \neq 5 \end{cases} \quad (\text{C.4})$$

1714

1715

1716

1717

$$F_3^{-1} = \begin{cases} F_n^{-1}, & \text{if } \text{typeRej}_{F_{heavy}} \text{ and } \text{typeRej}_{F_{lighter}} \geq 3 \\ F_{lighter}^{-1}, & \text{if } r_{right} \text{ is True, or } r_{all} \text{ is True and } \text{typeRej}_{F_{lighter}} \leq 2 \\ F_{heavy}^{-1}, & \text{otherwise} \end{cases} \quad (\text{C.5})$$

1718

1719

Let us define i_ℓ and i_u as follow :

1720

1721

1722

1723

1724

1725

1726

1727

$$\bullet i_\ell = \begin{cases} 0 & \text{if } r_{all} \text{ is True, or } i_{\ell, F_{heavy}} == 0 \\ i_{\ell, F_{heavy}} & \text{if } i_{\ell, F_{heavy}} > 0 \text{ and } r_{all} == \text{False} \\ i_{\ell, F_{lighter}} & \text{if } i_{\ell, F_{lighter}} > 0 \text{ and } r_{all} \text{ is True} \end{cases}$$

$$\bullet i_u = \begin{cases} n - 1 & \text{if } r_{all} \text{ is True or } i_{u, F_{heavy}} == n - 1 \\ i_{u, F_{heavy}} & \text{if } i_{u, F_{heavy}} < n - 1 \text{ and } r_{all} == \text{False} \\ i_{u, F_{lighter}} & \text{if } i_{u, F_{lighter}} < n - 1 \text{ and } r_{all} == \text{True} \end{cases}$$

1728

A different quantile function is used depending on the considered quantile, i.e.,

1729

1730

1731

1732

1733

$$\tilde{F}^{-1}(p) = \begin{cases} F_1^{-1}(p), & \text{if } p < \frac{i_\ell}{n} \\ F_2^{-1}(p), & \text{if } \frac{i_\ell}{n} \leq p < \frac{i_u+1}{n} \\ F_3^{-1}(p), & \text{if } \frac{i_u+1}{n} \leq p. \end{cases} \quad (\text{C.6})$$

1734

1735

This is a pseudo-quantile function because the monotonicity condition is not yet verified with the resulting \tilde{F} from (C.6).

1736

1737

Let us also define $C1$, $C1_{ceil}$, $C2$ and $C2_{ceil}$ as defined in Equations (C.1) and (C.2), as the corrections coefficient for respectively the lower and upper cutting index.

1738

1739

If the index is such that the correction coefficient cannot be defined (if the index is equal to 0 or $n - 1$ for respectively i_ℓ and i_u), then $C = 0$ and $C_{ceil} = +\infty$.

1740

1741

1742

Since the corrections (C.1) and (C.2) can not happen simultaneously, if $C > 0$, then $C_{ceil} = +\infty$, otherwise we let $C = 0$ if $C_{ceil} \neq +\infty$. The corrected-quantile function can then be defined as:

1743

1744

1745

1746

1747

1748

$$F^{-1}(p) = \begin{cases} \min(\tilde{F}^{-1}(p), C1_{ceil}) & \text{if } p < \frac{i_\ell}{n} \\ \min(\tilde{F}^{-1}(p) + C1, C2_{ceil}) & \text{else if } \frac{i_\ell}{n} \leq p < \frac{i_u+1}{n} \\ \tilde{F}^{-1}(p) + C1 + C2 & \text{otherwise.} \end{cases} \quad (\text{C.7})$$

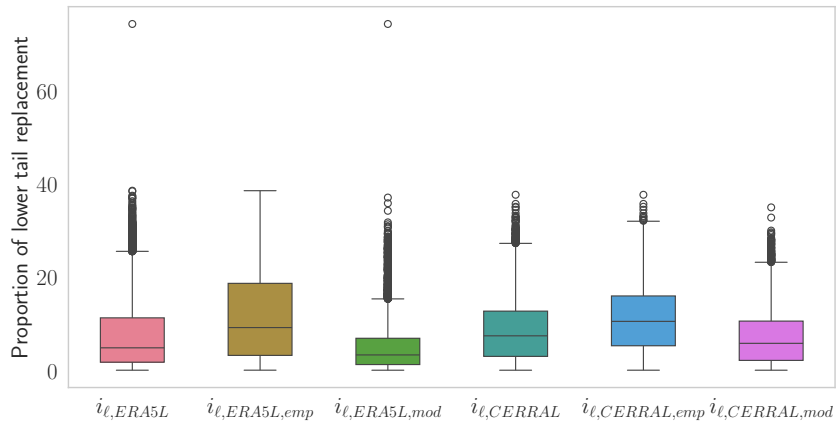
Given the properly quantile function defined in Equation (C.7), one can express the corresponding cdf given F_1, F_2 and F_3 in (C.3)-(C.5), the corrections $C1, C1_{ceil}, C2$ and $C2_{ceil}$ from Equations (C.1)-(C.2), and cutting indexes, i.e.,

$$F(x) = \begin{cases} F_1(x) & \text{if } x < F^{-1}(\frac{i_\ell}{n}) \\ F_2(x - C1) & \text{if } F^{-1}(\frac{i_\ell}{n}) \leq x < F^{-1}(\frac{i_u+1}{n}) \\ F_3(x - C1 - C2) & \text{if } F^{-1}(\frac{i_u+1}{n}) \leq x. \end{cases}$$

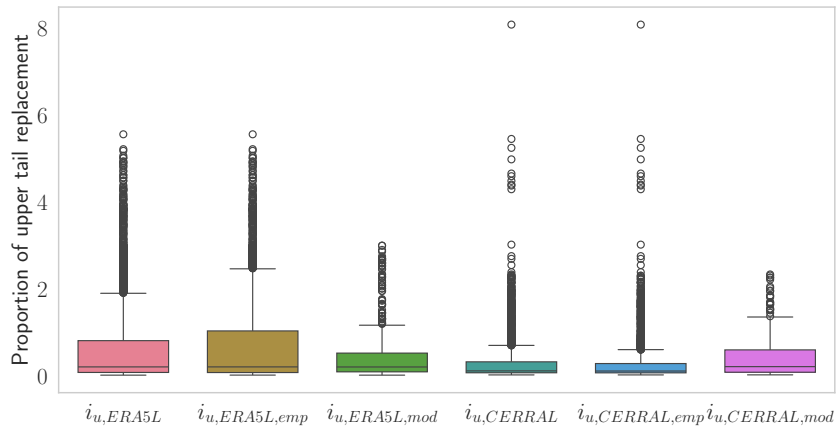
D Complementary figures

Boxplots of the proportion of upper and lower tail replacements are shown in Figure 28. In this figure, $i_{\ell,data,emp}$ and $i_{\ell,data,mod}$ (resp. $i_{u,data,emp}$ and $i_{u,data,mod}$) refer to the lower (resp. upper) cutting indexes introduced in Definition 1 of locations where respectively the empirical or the ExpW distributions were used to replace the lower (resp. upper) tail for a given time series. When *emp* or *mod* are not specified, i.e. $i_{\ell,ERA5L}, i_{\ell,CERRAL}, i_{u,ERA5L}, i_{u,CERRAL}$ in Figure 28, it refers to any cutting index of locations where a replacement occurred. We can see that for the upper tail, most replacements are done only on the last part of the upper tail, with at most 0.08% of the distribution replaced on the upper tail by an empirical distribution. On the lower tail, the proportion of the distribution replaced is higher. However, this point is less crucial for this particular study since small precipitations usually have a negligible impact on considered extreme rainfalls.

1795
 1796
 1797
 1798
 1799
 1800
 1801
 1802
 1803
 1804
 1805
 1806
 1807
 1808
 1809
 1810
 1811
 1812
 1813
 1814
 1815
 1816
 1817
 1818
 1819
 1820
 1821
 1822
 1823
 1824
 1825
 1826
 1827
 1828
 1829
 1830
 1831
 1832
 1833
 1834
 1835
 1836
 1837
 1838
 1839
 1840



(a) Proportion of lower tail replaced



(b) Proportion of upper tail replaced

Fig. 28: Proportion of replaced upper and lower tail for the model fitted on ERA5-L and CERRA-L.